Noname manuscript No.
(will be inserted by the editor)

Collisionless shocks in partly ionized plasma with cosmic rays: microphysics of non-thermal components

A.M. Bykov · M.A. Malkov · J.C. Raymond · A.M. Krassilchtchikov · A.E. Vladimirov

Received: date / Accepted: date

Abstract In this review we discuss some observational aspects and theoretical models of astrophysical collisionless shocks in partly ionized plasma with the presence of non-thermal components. A specific feature of fast strong collisionless shocks is their ability to accelerate energetic particles that can modify the shock upstream flow and form the shock precursors. We discuss the effects of energetic particle acceleration and associated magnetic field amplification and decay in the extended shock precursors on the line and continuum multi-wavelength emission spectra of the shocks. Both Balmer-type and radiative astrophysical shocks are discussed in connection to supernova remnants interacting with partially neutral clouds. Quantitative models described in the review predict a number of observable line-like emission features that can be used to reveal the physical state of the matter in the shock precursors and the character of nonthermal processes in the shocks. Implications of recent progress of gamma-ray observations of supernova remnants in molecular clouds are highlighted.

Keywords collisionless shocks · radiative shocks · supernova remnants · gamma-rays

A.M. Bykov
A.F. Ioffe Institute for Physics and Technology, 194021, St.Petersburg, Russia
E-mail: byk@astro.ioffe.ru

M.A. Malkov
University of California, San Diego, La Jolla, California 92093, USA
E-mail: mmalkov@ucsd.edu

J.C. Raymond
Center for Astrophysics, 60 Garden St, Cambridge, MA 02138, USA
E-mail: jraymond@cfa.harvard.edu

A.M. Krassilchtchikov
A.F. Ioffe Institute for Physics and Technology, 194021, St.Petersburg, Russia
E-mail: kra@astro.ioffe.ru

A.E. Vladimirov
Stanford University, Stanford, CA 94305, USA E-mail: avladim@stanford.edu

1 Introduction

Plasma flows with collisionless shocks are found in a number of energetic space objects, such as supernova remnants (SNRs) interacting with atomic or molecular clouds (McKee and Hollenbach 1980; Draine and McKee 1993; Heng 2010), Herbig-Haro objects (Hartigan et al. 1987; Giannini et al. 2008; Teşileanu et al. 2009), winds from protostars and young stellar objects (Massi et al. 2008), recurrent novae (Evans et al. 2007; Bode et al. 2007; Tatischeff and Hernanz 2007), and also in accretion flows in the vicinities of galactic nuclei (Farage et al. 2010).

Already in the early studies of Raymond (1979) and Shull and McKee (1979) the ionization state of the pre-shock flow was recognized as an important feedback parameter that influences the dynamics of the flow, and hence, the spectrum of continuum and line emission produced in the post-shock zone. While Raymond (1979) took the pre-shock ionization state as a free parameter, Shull and McKee (1979) included the ionizing flux from the post-shock to obtain a pre-shock ionization state self-consistently with the temperature and ionization profiles in the post-shock. Dopita and Sutherland (1996) furthered the calculation of the precursor photoionization, and presented emission line spectra assuming an equilibrium with the ionizing flux from the shock.

Recent observations of forward shocks in galactic SNRs indicate a substantial role of nonthermal components in the energy budgets of post-shock flows (e.g., Helder et al. 2012). While the fraction of the energy dissipated in the shock itself may be smaller for slower radiative shocks, the enhanced radiative cooling in their post-shocks leads to stronger compression so that cosmic ray and magnetic pressure can dominate over thermal pressure in the zones where most of the observed optical and IR emission is produced. There is also a growing consensus on that in both parallel and perpendicular shocks the diffusing cosmic rays may generate unstable plasma currents and turbulence in the pre-shock zone, thus allowing for efficient particle acceleration, shock modification, and substantial enhancement of the total compression ratio (Blandford and Eichler 1987; Jones and Ellison 1991; Malkov and Drury 2001; Bell 2004; Bykov et al. 2012). Raymond et al. (1988b) analyzed a shock in the Cygnus Loop SNR and found that the nonthermal pressure exceeds the thermal pressure by an order of magnitude in the zones where the [S II] lines are formed, though they were unable to distinguish between magnetic and cosmic ray contributions. Neutral particles could affect the processes of particle acceleration (e.g., Draine and McKee 1993; O'C Drury et al. 1996; Malkov et al. 2005; Blasi et al. 2012; Inoue et al. 2012; Ohira 2012; Helder et al. 2012; Morlino et al. 2012a), magnetic field amplification and plasma heating in the upstream region (e.g., Bykov and Toptygin 2005; Reville et al. 2007).

In this paper we review physical mechanisms governing evolution of supersonic and superalfvenic flows with collisionless shocks in partially ionized plasmas with nonthermal components. Section 2 describes the photoionization precursors that help determine the neutral fraction of the pre-shock gas. In Section 3 Hα signatures of interaction of neutral particles with fast shocks are depicted. In Section 4 we discuss specific plasma heating processes due to dissipation of CR-driven magnetic fluctuations in the shock precursor. A consistent pre-shock ionization structure is given in Section 5 with an aim to emphasize processes that critically influence optical and IR spectra emitted from the flows. The escape of accelerated energetic particles may affect the gas compression in the shock upstream and plasma temperature in the downstream resulting in formation of radiative shocks of velocities that may well exceed that of the adiabatic shocks. We discuss the line spectra of radiative shocks modified by CR acceleration

effect in Section 5. Specific features of CR acceleration in supernova remnants interacting with molecular clouds are discussed in Section 6 and their gamma-ray emission spectra are outlined in Section 7. A brief summary is given in Section 8.

2 Photoionization Precursors

The neutral fraction in the pre-shock gas often depends on photoionization by radiation from the shock itself. There are two regimes, non-radiative shocks are those in which gas is heated at the shock but does not have time to radiatively cool, while radiative shocks radiatively cool from the post-shock temperature, efficiently converting their thermal energy into radiation. Naturally, the latter produce more ionizing photons if the post-shock temperature exceeds about 150,000 K. The scale of the photoionization precursor is given by the photoabsorption cross section of hydrogen and the neutral density in the pre-shock gas, so it is typically 10^{18} or 10^{19} cm. In supernova remnants, shocks faster than 300 km/s are typically nonradiative, while slower shocks are generally radiative.

Non-radiative shocks produce some ionizing photons because some of the atoms passing through the shock are excited before they are ionized in the hot post-shock plasma. In particular, at high temperatures each He atom produces a few photons in the He I 58.4 nm and He II 30.4 nm lines. Since He makes up about 10% of the gas, the pre-shock region will be by 30% to 40% ionized by these photons. EUV emission from the hot post-shock gas can further ionize the plasma. The photons are relatively energetic, so they heat the gas to around 16,000 K. Emission from such precursors outside Tycho's SNR and N132D were reported by Ghavamian et al. (2000) and Morse et al. (1996).

As mentioned above, and as described more fully in Section 5, radiative shocks faster than about 100 km/s produce large fluxes of ionizing photons, and those above about 120 km/s produce enough photons to fully ionize H in the pre-shock gas. However, it should be kept in mind that the equilibrium between pre-shock ionization state and ionizing flux from the shock, as assumed in Shull and McKee (1979); Dopita and Sutherland (1996), does not always hold. In particular, an SNR shock can evolve more rapidly than the recombination time in the pre-shock gas, or the transverse scale of the shock may be smaller than the upstream photon mean free path, as it is in a Herbig-Haro object (Raymond et al. 1988a).

3 Interaction of Neutrals with Fast Shocks: Hα Signatures

Neutral H atoms are not affected by the electromagnetic fields or plasma turbulence in a collisionless shock. They pass freely through the shock transition, whose thickness is given by the ion inertial length or the proton gyroradius, which are typically $\sim 10^8$ cm in the interstellar medium. However, they become ionized in a hot downstream plasma but, because of the low ISM densities, they travel $\sim 10^{14}$-10^{15} cm downstream before it happens. This is smaller than electron-proton thermal equilibration scales, and therefore, the emission from neutrals may contain information about the post-shock conditions of electrons and ions before relaxation.

The hydrogen atoms are ionized either by collisions with protons and electrons or by a charge exchange with protons. The latter process produces a population of neutrals with a velocity distribution similar to that of the post-shock protons and, when they are

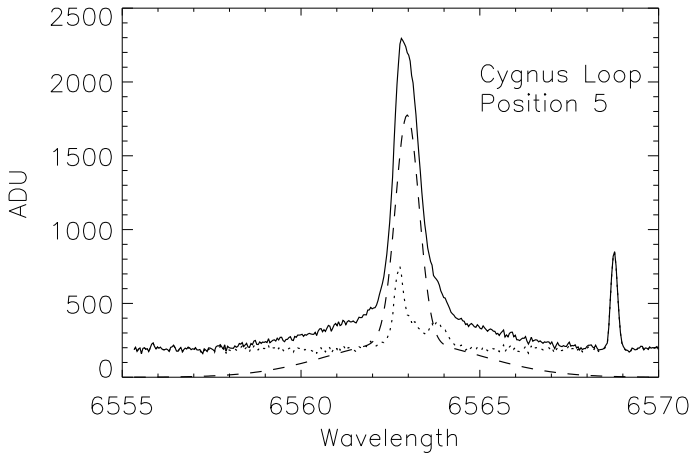

Fig. 1 Hα profile of a 350 km/s shock at the outer edge of the Cygnus Loop, obtained with the HECTOCHELLE spectrograph on the MMT. The narow component is 30 km/s wide (FWHM), and the broad component is 225 km/s wide. Full line is the observation, dashed line is the Hα from the filament, and dotted line is the sky background. The feature near 6569Å is an airglow line.

excited, they produce broad Lyman and Balmer emission lines whose velocity widths are comparable to the shock speed (Chevalier and Raymond 1978; Raymond 1991; Heng 2010; France et al. 2011). Neutrals that are excited before the charge transfer produce a narrow component whose width is given by the pre-shock temperature (see Figure 1). The broad-to-narrow intensity ratio indicates the electron temperature, while the broad component width directly measures the proton temperature. Thus one can determine the electron-ion temperature ratio at the shock (Ghavamian and Schwarz this volume). Consequently, the Hα profile provides both the post-shock temperature and T_e/T_p ratio. These quantities can be used to determine the shock speed (Smith et al. 1994; Hester et al. 1994; Ghavamian et al. 2001; van Adelsberg et al. 2008). Under the assumption that only a small fraction of the shock energy goes into cosmic rays, the shock speed can be determined from the post-shock proton and electron temperature using momentum and energy conservation laws. However, if cosmic ray acceleration is efficient, then T_e and T_p combined with a model of efficient cosmic ray acceleration can yield a shock velocity (Helder et al. 2009) though there is some ambiguity due to a contribution to the narrow component from a shock precursor (see Section 3.2).

The Balmer line profiles can also indicate more exotic plasma processes. First, if the post-shock proton velocity distribution is not Maxwellian, it will leave an imprint on the broad component line profile. Second, the strength and width of the narrow component can indicate heating and excitation in a shock precursor. We discuss signatures of these departures from a simple shock picture.

3.1 Non-Maxwellian Velocity Distributions

If cosmic rays are accelerated in SNR shocks, the particle velocity distribution is manifestly non-Maxwellian, taking the form of a Maxwellian core with a power law tail. Such distributions are conveniently parameterized with the κ function (Pierrard and Lazar 2010). The κ distribution approaches a Maxwellian as κ approaches infinity, while the power law tail becomes harder and includes a larger fraction of the particles as κ approaches its lower limit of 1.5.

A different sort of departure from a Maxwellian can arise because of the neutral atoms themselves. When a neutral becomes ionized, it is moving at 3/4 the shock speed with respect to the downstream plasma and magnetic field (assuming a shock compression factor of 4). It therefore behaves like a pickup ion in the solar wind (Gloeckler and Geiss 2001). Initially, all these newly-formed protons have the same velocity with respect to plasma in which they are immersed. This velocity separates into a gyration speed around the magnetic field plus a component along the field, and since all the particles have the same initial velocity (assuming that the shock speed is large compared to the pre-shock thermal speed), they form a ring beam in velocity space. That distribution is unstable, and it rapidly evolves into a bispherical shell in velocity space, a lens-like shape that depends on the ratio of the Alfvén speed to the initial particle speed (Williams and Zank 1994). The protons in the bispherical shell can then experience charge transfer to produce observable neutrals. The process of ionization, interaction with the magnetic field, and subsequent re-neutralization is the same sequence of events that produce the "IBEX ribbon" seen in H atoms from beyond the heliopause (McComas et al. 2009).

The Hα profiles produced by the pickup ion process were computed by Raymond et al. (2008). The neutral fraction in the pre-shock gas must be substantial in order to produce the Balmer line filaments seen at the edges of some supernova remnants and pulsar-wind nebulae, and therefore the neutrals can have a significant effect on the shock structure. Heng et al. (2007) computed the gradual transition over the charge transfer length scale, but found little effect on the overall dynamics. Ohira et al. (2009) examined the streaming instabilities created by the relative motion of the post-shock plasma and the protons created downstream (this effect is stronger in parallel shocks) and predicted substantial amplification of the magnetic field. Raymond et al. (2008) calculated the wave energy produced as the ring beam relaxes to a bispherical distribution, and showed that it could significantly affect the electron temperature if the waves couple efficiently to electrons. Ohira and Takahara (2010) considered the modification of the shock structure, in particular weakening of the subshock, and the effects on the cosmic ray spectrum.

The observational evidence for any departure of the proton distribution from a Maxwellian is still ambiguous. For nearly all the observed Hα broad components Gaussian fits are adequate, but in general the lines are so faint that even the determination of the line width is subject to large statistical uncertainty. A very deep exposure of a bright knot in Tycho's SNR yielded the only profile that shows a clear non-Gaussian broad component, but there are several possible interpretations (Raymond et al. 2010). The departure could be attributed to a power law tail, however, the slope of this tail is very hard, which indicates extremely efficient particle acceleration. The profile could also be matched by the combination of a pickup ion component with an ordinary Maxwellian component, though this requires a fairly high pre-shock neutral fraction. A third possibility is that some of the neutrals in the shock precursor aquire a kinetic temperature

about 1/2 of the post-shock temperature. Clearly, this implies a precursor to be both hot and thick. Finally, one could produce the observed profile by adding contributions from separate shocks along the line of sight. However, this possibility would require quite a large velocity difference, and therefore a significant density contrast between the two regions. At higher shock speeds, the velocity dependence of the charge transfer cross section can distort the profile (Heng and McCray 2007; Heng et al. 2007), but that is unlikely to account for the Tycho observations.

3.2 Shock Precursors

The precursor of a collisionless shock wave is a region upstream of the shock transition in which the plasma conditions (velocity, density, temperature, magnetic fields, ionization state) are affected by photons or superthermal particles streaming ahead of the shock front.

Shock wave precursors can be produced by ionizing photons emerging from the downstream region or by broad component neutrals that leak back through the shock. Additionally, in shocks that produce accelerated super-thermal charged particles, precursors can be produced as a consequence of this acceleration process. We first consider the observational evidence for precursors, then the physics of the three mechanisms and the implications for system parameters.

The first evidence for precursors to SNR shocks came from the observation that the widths of the Hα narrow components in several shocks were unexpectedly large. Smith et al. (1994) measured narrow component widths of 25-58 km/s in four LMC Balmer-dominated remnants, and Hester et al. (1994) found a 28-35 km/s width in a Cygnus Loop shock. These line widths correspond to temperatures of about (2–7)$\times$ 10^4 K, and in static equilibrium, hydrogen is fully ionized at those temperatures. Thus Smith et al. (1994) and Hester et al. (1994) concluded that the gas must be heated in a narrow region ahead of the shock. The region must be thick enough so that charge transfer can heat the neutrals, but thin enough that the neutrals do not become ionized. Subsequent observations have revealed line widths of 44 km/s in Tycho's SNR (Ghavamian et al. 2000) and 30-42 km/s in RCW 86 and Kepler's SNR, with only SN 1006 showing a narrow component width compatible with a temperature of 10,000 K and a significant neutral fraction (Sollerman et al. 2003). Nikolić et al. (2013) have presented Integral Field Unit spectra of a section of the Hα filament in SN 1006, and they have found that a precursor makes a substantial contribution to the narrow component of Hα.

The precursor thicknesses must be about $1''$ in order for the neutrals to be heated, and they have been spatially resolved in the Cygnus Loop (Fesen and Itoh 1985; Hester et al. 1994) and in Tycho's SNR (Lee et al. 2007, 2010).

3.3 Physical Interpretation of Shock Precursors

Three ideas have been put forward to explain observed shock precursors, a photoionization precursor, a cosmic ray precursor, or a precursor created by fast neutrals leaking from the post-shock region out ahead of the shock.

The photoionization precursor heats the electrons, and it has a very large length scale. In non-radiative shocks, each He atom passing through the shock produces about

2 He II λ304 photons and 1 to 2 He I λ584 photons. These photons can ionize about 30% of the pre-shock hydrogen, and because the photons are relatively energetic they deposit considerable heat in the electrons. Such a precursor has been reported ahead of Tycho's supernova remnant (Ghavamian et al. 2000). However, because they heat the electrons and extend over large length scales, photoionization precursors do not explain the observations discussed in Section 3.2.

A precursor is an integral part of diffusive shock acceleration models, in which an MHD turbulence scatters energetic particles moving away from the shock back towards it (Blandford and Eichler 1987). Its thickness is given by κ_{CR}/V_s, where κ_{CR} is the cosmic ray diffusion coefficient. While κ_{CR} is of order 10^{28} cm^2/s in the ISM, it must be somewhere closer to the Bohm limit near the shock in order for particles to reach high energies, perhaps 10^{24} cm^2/s. That implies a precursor thickness of order 10^{16} cm, or about $1''$ for nearby SNRs. The heating in such a precursor can occur by dissipation of the turbulence itself. It will be especially strong if neutrals are present to provide ion-neutral wave damping, which can limit the wave intensity and therefore the highest particle energies reached (Draine and McKee 1993; O'C Drury et al. 1996). The heating will also be strongest in shocks that accelerate cosmic rays efficiently. If the precursor heating is strong, it can reduce the Mach number of the subshock, changing the cosmic ray spectrum and pressure (see, e.g., Vladimirov et al. 2008; Wagner et al. 2009; Vink et al. 2010).

Several theoretical models have considered the effects of neutral-ion collisions on the dynamics and temperature of the precursor. Boulares and Cox (1988) computed the heating and ionization in cosmic ray precursors for the modest shock speeds in the Cygnus Loop. Ohira and Takahara (2010) considered neutrals interacting in the precursor, treating them as pickup ions. The pickup ions can strongly heat the plasma and affect the jump conditions at the subshock, and because of their high velocities they are preferentially injected into the diffusive acceleration process. Raymond et al. (2011) computed the temperature and density structures of precursors and the resulting Hα emission. If cosmic ray acceleration is efficient, the Hα profiles are strongly modified, both in broadening the narrow component and decreasing the broad-to-narrow intensity ratio. The Hα profiles reported so far are consistent with moderate ratios of cosmic ray pressure to gas pressure, but not with ratios above about 0.4. Most recently, Morlino et al. (2012b) have included a parameterized form of wave damping along with wave growth due to the cosmic ray pressure gradient for a more self-consistent treatment of the cosmic ray spectrum in the presence of neutrals and the resulting Hα profiles. They also find that an intermediate velocity width component can arise, similar to the complex profiles predicted in Raymond et al. (2011).

The other suggested mechanism for producing a precursor is leakage of some of the broad component neutrals out through the shock front. These neutrals have the thermal speeds of post-shock protons and a bulk speed of $V_S/4$ away from the shock. A significant fraction of them, of order 10%, can overtake the shock, and of course they pass through (Smith et al. 1994; Hester et al. 1994). They carry a substantial amount of energy, but it is unclear how much of that energy heats the precursor plasma. Lim and Raga (1996) found that they became ionized to form a beam of fast protons, but that the protons are swept back through the shock without transferring much energy to the bulk plasma. Ohira (2012) constructed four-fluid models and showed that the leaking particles decelerate the upstream flow and affect the subshock compression ratio. Blasi et al. (2012) computed the energy and momentum exchange between neutrals and ions on both sides of the subshock, using a procedure like that of Heng et al.

(2007) to compute the neutral velocity distribution and the flux of neutrals from the post-shock region to the precursor. Then they used the resulting precursor structure to compute spectral slopes of accelerated particles. The authors accounted for neutrals ionization by protons only, though photo ionization processes can affect the ionization states for some shock parameter space. Morlino et al. (2012a) used the kinetic simulations of Blasi et al. (2012) to calculate the Hα emission produced in the precursor. Its intensity depends on the poorly constrained efficiency of electron-ion equilibration, since the heat is deposited in the ions, but the electrons excite the line. They find that the profiles can deviate strongly from Gaussian and that in some circumstances an intermediate width component can arise. They suggest that this could explain profiles observed in Tycho's SNR. Morlino et al. (2012b) have extended this work by including the cosmic rays along with the neutrals that escape upstream through the shock.

4 CR precursor heating and the post-shock temperature

Models of collisionless shocks with large sonic and Alfvénic Mach numbers ($\mathcal{M}_{\rm s} >> 1$ and Alfvénic $\mathcal{M}_{\rm a} >> 1$) show that, through the first-order Fermi acceleration mechanism, a small minority of particles could gain a disproportionate share of the energy and populate the high energy tail of particle distribution. The energetic particles can penetrate far into the shock upstream gas, to create an extended shock precursor illustrated in Figure 2. The cold gas in the shock precursor is decelerated and pre-heated by fluctuating magnetic field dissipation on a scale that is about $c/v_{\rm sh}$ times larger than a mean free path of an energetic particle λ_*. Shocks in collisionless supersonic flows produce a complex multi-scale structure of the relaxation region with an extended precursor and sub-shock of a modest sonic Mach number $\mathcal{M}_{\rm sub} \sim 3$.

This section discusses theoretical models of strong collisionless shocks and their implications for the observations of shock precursors discussed in Section 3.2.

4.1 The structure of a non-linear shock precursor in the presence of self-generated MHD turbulence

Consider a strong, plane-parallel collisionless shock in a plasma of finite $\beta = \mathcal{M}_{\rm a}^2/\mathcal{M}_{\rm s}^2$ (β is the ratio of plasma pressure to magnetic pressure). The distribution function of nonthermal particles and the bulk flow profile in the shock upstream region are sensitive to both the total upstream compression ratio $r_{\rm tot}$ and the subshock Mach number $\mathcal{M}_{\rm sub}$. Direct numerical simulations of the CR-modified shock by particle-in-cell technique are nonfeasible by now because of the wide dynamical range of the simulation that requires extreme computing resources. Nevertheless, an approximate iterative approach (e.g., within the Monte Carlo model discussed in Vladimirov et al. (2008) or semi-analytical kinetic models developed by Malkov (1997); Amato and Blasi (2006)) can be used to derive the steady-state distribution function consistent with the shock compression. These approximate models assume some diffusion model and parameterize the microphysical processes of magnetic field amplification and plasma heating. The exact calculation of the CR escape flux $Q_{\rm esc}$ that determines the total upstream compression ratio $r_{\rm tot}$ can be performed only in fully nonlinear self-consistent simulations. The Monte Carlo model of Vladimirov et al. (2008) describes the escape of particles from the shock with an assumed free escape boundary far upstream of the

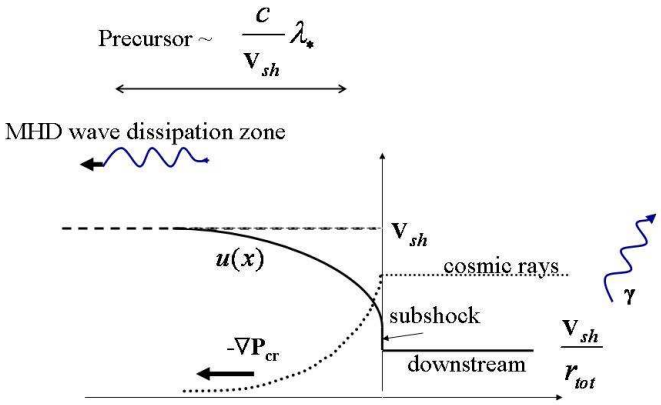

Fig. 2 A schematic view of a CR-modified shock propating to the right.

shock. The distance to the free escape boundary is a free parameter of the simulation that controls the maximum energy of accelerated particles and the escaping CR flux (see Ellison et al. (1996) for more details of this method).

The role of accelerated particles in the shock precursor depends on the poorly known mechanisms with which energetic particles can transfer energy to the thermal pool. However, in order to numerically estimate the impact of such a process, Vladimirov et al. (2008) parameterize the rate of plasma heating upstream. In order to do that, they assume that CR particles produce, through the resonant CR streaming instability, strong fluctuations of magnetic fields upstream of the shock. Another assumption in the model is that these fluctuations are immediately dissipated into the heat of the thermal gas, and that the rate of turbulence dissipation is proportional to the rate of turbulence generation. The dimensionless parameter α_H in the model is the ratio of dissipation to generation rate. Figure 3 adopted from Vladimirov et al. (2008) shows the self-consistently calculated flow speed, effective magnetic field and the temperature in the precursor of a strong shock with turbulence dissipation for several values of α_H. This work demonstrated that even a small rate of turbulence dissipation can significantly increase the gas temperature in the precursor, and thus increase the rate of injection of thermal particles. At the same time, the spectrum of high energy particles is only modestly affected by dissipation in these simulations.

In a follow-up work of Vladimirov et al. (2009) the effect of the microphysics of the fluctuating magnetic fields in the shock precursor was modeled in a more physically realistic manner. That work used the balance equation of the turbulence spectral energy density

$$\frac{\partial W}{\partial t} + \mathbf{u}\,\nabla_{\mathbf{r}} W + \nabla_{\mathbf{k}} \mathbf{\Pi} = S(x,\mathbf{k}) - L_{\rm turb}. \qquad (1)$$

Here $L_{\rm turb}(x,\mathbf{k})$ represents the dissipation of turbulence, the turbulence energy injection rate is $S(x,\mathbf{k}) = \gamma(x,\mathbf{k})W(x,\mathbf{k},t)$, and $\gamma(x,\mathbf{k})$ is the rate of wave energy amplification by the CR-driven instabilities (see for a discussion Bykov et al. 2012; Schure et al.

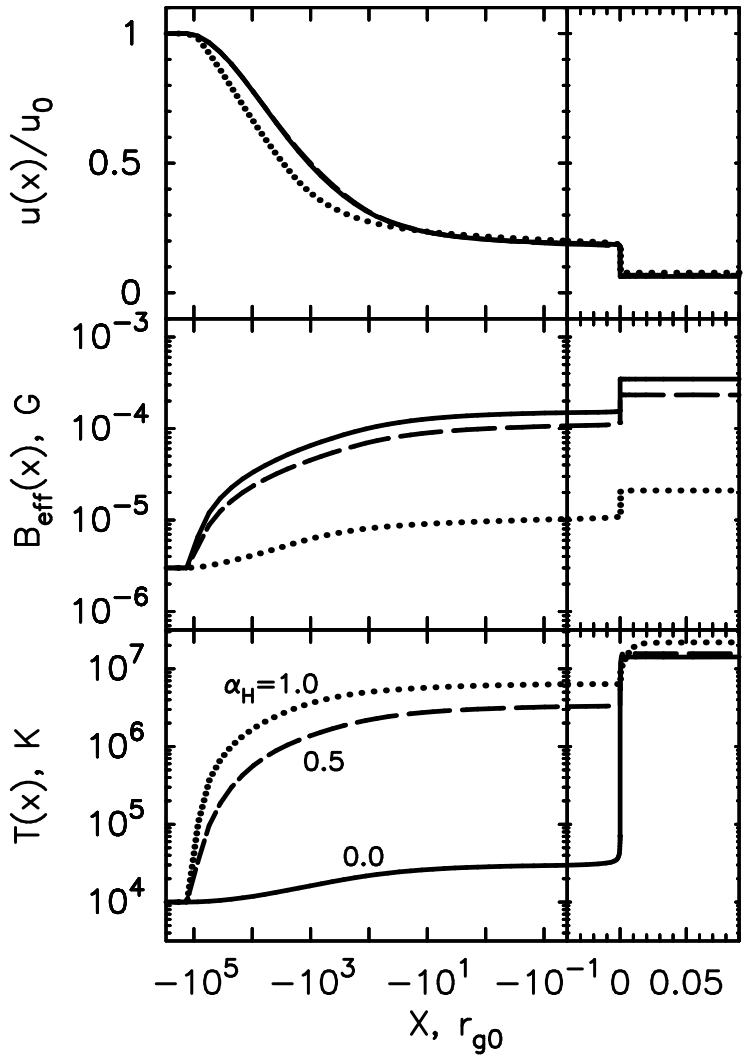

Fig. 3 The profile of a CR-modified shock simulated with Monte-Carlo nonlinear DSA model by Vladimirov et al. (2008). The solid, dashed and dotted lines correspond, respectively, to a fraction, $\alpha_H = 0$, 0.5 and 1.0, of the magnetic energy that goes into heating of the thermal gas. The plotted quantities are the bulk flow speed $u(x)$, the effective amplified magnetic field $B_{\rm eff}(x)$ and the thermal gas temperature $T(x)$. The shock is located at $x = 0$.

2012). The fastest short-wavelength CR-driven instability studied by Bell (2004) has the following growth rate for the wavevector along the mean magnetic field:

$$\gamma_{\rm CR} = 2v_A k_\parallel \sqrt{\frac{k_c}{k_\parallel} - 1}, \quad \text{for} \quad 1/r_{\rm g1} < k < k_c, \tag{2}$$

where $v_A(x) = B_0/\sqrt{4\pi\rho(x)}$ is the Alfvén speed, c is the speed of light, B_0 is the far upstream magnetic field directed towards the shock normal, $\rho(x)$ is the thermal

plasma mass density, $r_{\rm g1}(x)$ is the gyroradius of the least energetic current generating CR, the critical wavenumber $k_c(x) = 4\pi j_d(x)/(cB_0)$, and the local diffusive electric current of CRs responsible for the instability, $j_d(x)$, is determined via a Monte Carlo simulation. The turbulence energy density flux $\mathbf{\Pi}(\mathbf{r}, \mathbf{k}, t)$ describes anisotropic cascading, i.e., the transfer of turbulence energy from long to short wavelengths (Kolmogorov type cascade) as well as the inverse cascade (see, e.g., Monin and Iaglom 1975; Zhou and Matthaeus 1990; Verma 2004; Zhou 2010).

Modeling the balance, spectral distribution, and dissipation of turbulence energy with equation (1) allows us to construct more physically realistic models of shock precursors and account for the Balmer line observations discussed in Section 3. This equation must be supplemented by theoretical models of the growth, dissipation and spectral flux of MHD turbulence produced by CRs. Sections 4.2 and 4.3 discuss some of the ongoing work in this area.

4.2 MHD turbulence damping in partially ionized plasmas

Ion-neutral collisions may dominate the frictional damping of strong magnetic oscillations in a cold photo-ionized plasma ($T \sim 2 \times 10^4$ K) of a precursor of a CR-modified shock (Draine and McKee 1993; O'C Drury et al. 1996). In a cold partially ionized plasma the generalized Ohm's law (see, e.g., Braginskii 1965; Cowling 1976)

$$\mathbf{E} + \frac{1}{c}\mathbf{u} \times \mathbf{B} = \frac{\mathbf{j}}{\sigma} + \frac{1}{n_i e c}\mathbf{j} \times \mathbf{B} + \frac{F^2 \tau_{ia}}{n_i m_i c^2}\mathbf{B} \times (\mathbf{j} \times \mathbf{B}). \tag{3}$$

results in enhanced effective magnetic diffusion ν_{ef} in the induction equation

$$\nu_{ef} = \frac{c^2}{4\pi\sigma_\perp^{ef}}, \tag{4}$$

where

$$\frac{1}{\sigma_\perp^{ef}} = \frac{1}{\sigma} + \frac{F^2 B^2}{n_i m_i c^2}. \tag{5}$$

Here F is the mass fraction of the neutrals, τ_{ia} is the mean time between the ion-neutral collisions. The neutrals in cold magnetized plasma of supernova shock precursors may strongly affect both the growth and the dissipation of CR-driven waves (see, e.g., Bykov and Toptygin 2005; Marcowith et al. 2006; Reville et al. 2007). In a precursor of a quasi-parallel shock the CR-driven turbulence is basically incompressible and the energy dissipation rate $\mathit{\Gamma}^{in}$ in the low β limit can be estimated as

$$\mathit{\Gamma}^{in} = \sigma_\perp^{ef}\, k_\parallel^2,$$

while the ion-neutral dissipation of the compressible fluctuations that are associated with long-wavelength CR-driven oblique wave instabilities (see, e.g., Bykov et al. 2011; Schure et al. 2012) are determined by

$$\mathit{\Gamma}^{in} = \sigma_\perp^{ef}\, k^2.$$

The magnetic turbulence dissipation term in Eq. (1) due to effective magnetic diffusivity (Joule dissipation) is determined by

$$L^{in}_{\rm turb}(x, \mathbf{k}) = \nu_{ef} k^2 W(x, \mathbf{k}, t). \tag{6}$$

To characterize a fraction of the magnetic energy dissipated in the precursor of a CR-modified shock it is instructive to estimate the minimal wavenumber k_m of the fluctuations to be strongly dissipated by ion-neutral friction while advecting through the CR-shock precursor of the scale length $L_{CR} \sim c/v_{\rm sh}\,\lambda_*$ as it is illustrated in Figure 2, where

$$\nu_{ef}\,k_m^2 \times \frac{L_{CR}}{\rm v_{sh}} = 1. \tag{7}$$

Then the maximal wavelength to be damped is

$$\lambda_m = 2\pi/k_m \approx 2\pi\,F\,\mathcal{M}_{\rm a}^{-1} \times \sqrt{c\tau_{ia}\lambda_*}. \tag{8}$$

For a strong supernova shock of $\mathcal{M}_{\rm a} \approx 100$ and $F \approx 0.1$ one may get $\lambda_m \lesssim 10^{15}$ cm. Note, however, that the length λ_m is comparable to the ion-neutral collision length that is $\sim [F\,n_i\,\sigma_{in}]^{-1}$, if the ion number density in the precursor $n_i \lesssim 1$ cm^{-3}. Depending on the spectral shape of the CR-driven magnetic turbulence in the shock precursor, the dissipated fraction ranges from a few percent for a Kolmogorov-type spectrum to about 10% for the flatter spectra of strong turbulence. We neglected here the MHD wave dissipation due to the thermal conduction and viscosity assuming a cold plasma case (see, e.g., Braginskii 1965, for a thorough discussion). The magnetic power dissipated by the ion-neutral collisions in the low β plasma mainly heats ions. The collisional damping discussed above results in a true irreversible conversion of the magnetic turbulence free energy into the thermal plasma energy. To the contrary, the collisionless turbulence dissipation processes that we are going to discuss below can heat electrons, thus being not completely irreversible. The collisionless heating process just increases the energy of quasi-thermal plasma components, but in general some collisionality (e.g., Ramos 2011) is required to increase the entropy and to reach the equilibrium distributions of plasma species.

4.3 Collisionless heating of ions and electrons by magnetic turbulence

The CR-driven turbulence source $S(x, \mathbf{k})$ in the shock precursor is expected to be anisotropic in $\mathbf{k}$. The fast CR-current driven instability of Bell (2004) as well as the long-wavelength instability of Bykov et al. (2011) in the Bohm diffusion regime are mainly amplifying the modes with the wavevectors along the local magnetic field. The acoustic instability of Drury and Falle (1986) driven by the CR-pressure gradient is also anisotropic. The strong anisotropy of the magnetic turbulence is observed in the solar wind where the outward flux significantly exceeds the ingoing one.

The solar wind is one of the best laboratories to study anisotropic magnetic turbulent dissipation and collisionless plasma heating (see, e.g., Leamon et al. 1998; Sahraoui et al. 2009; Petrosyan et al. 2010; Alexandrova et al. 2011). Recently, Sahraoui et al. (2009) reported *Cluster* spacecraft measurement providing direct evidence that the dissipation range of magnetofluid turbulence in the solar wind extends down to the electron scales. Namely, they found two distinct breakpoints in the magnetic spectrum at frequencies $f_p = 0.4$ Hz and $f_e = 35$ Hz, which correspond, respectively, to the Doppler-shifted proton and electron gyroscales. Below f_p, the spectrum follows a Kolmogorov-type scaling of power-law index about -1.62. For $f_p < f < f_e$ a second inertial range with a scaling index -2.3 was established. Above f_e the spectrum has a steeper power law -4.1 down to the noise level of the *Cluster* detectors. The authors advocated a good

agreement of the results with theoretical predictions of a quasi-two-dimensional cascade into Kinetic Alfvén Waves (KAW). Chen et al. (2012) presented a measurement of the scale-dependent, three-dimensional structure of the magnetic field fluctuations in the inertial range of the solar wind turbulence. The Alfvén -type fluctuations are three-dimensionally anisotropic, with the sense of this anisotropy varying from large to small scales. At the outer scale, the magnetic field correlations are longest in the local fluctuation direction. At the proton gyroscale, they are longest along the local mean field direction and shortest in the direction perpendicular to the local mean field and the local field fluctuation. The compressive fluctuations are highly elongated along the local mean field direction, although axially symmetric in the perpendicular direction. Their large anisotropy may explain why they are not heavily damped in the solar wind by the Landau damping.

Anisotropic wavenumber spectra that are broader in wavenumber perpendicular to the background magnetic field than in the parallel one are expected even in the symmetric MHD case studied by Goldreich and Sridhar (1995) where the oppositely directed waves carry equal energy fluxes. The main features of the the symmetric (but anisotropic) MHD turbulence model by Goldreich and Sridhar (1995) are:

(i) a critical balance between the linear wave mode periods and their nonlinear turnover timescales in the inertial-interval energy spectrum;

(ii) the 'eddies' are elongated in the direction of the field on small spatial scales with the scaling $k_{\|} \propto k_0^{1/3} k_{\perp}^{2/3}$, where k_0 is the wavenumber corresponding to the outer scale of the turbulence.

The three-dimensional simulations by Cho and Lazarian (2004) revealed the basic features of the Goldreich and Sridhar (1995) model in the electron magnetohydrodynamic turbulence. The kinetic Alfvén wave and whistler fluctuations are likely to make an important contribution to the turbulence below the proton gyroscale (see, e.g., Gary et al. 2012; Saito and Gary 2012; Boldyrev and Perez 2012; Mithaiwala et al. 2012). Particle-in-cell simulations show that the anisotropic whistler turbulence heats the electrons in the parallel direction as predicted by the linear theory and that in the low β plasmas the magnetic wavenumber spectrum becomes strongly anisotropic with spectral index in the perpendicular direction close to -4 (see, e.g., Gary et al. 2012; Saito and Gary 2012). Microscopic two-dimensional particle-in-cell simulations of whistler turbulence were carried out by Saito and Gary (2012) in a collisionless homogeneous magnetized plasma to study the electron and ion heating dependence on the plasma magnetization parameter β. They demonstrated that at higher values of β the magnetic energy cascade in the perpendicular direction becomes weaker and leads to more isotropic wavenumber spectra. The electron energy ratio between parallel and perpendicular components becomes closer to unity at higher β. Three-dimensional particle-in-cell plasma simulations of decay of initial long wavelength whistler fluctuations into a broadband, anisotropic, turbulent spectrum at shorter wavelengths via a forward cascade were performed by Gary et al. (2012). The simulations demonstrated a picture qualitatively similar to that in 2D but somewhat stronger anisotropy of the resulting 3D turbulence comparing to the similar 2D runs. They showed a clear break in the perpendicular wavenumber spectra qualitatively similar to that measured in the electron scale fluctuations in the solar wind. Earlier Quataert (1998) and Quataert and Gruzinov (1999) discussed the beta-dependence of particle heating by turbulence in advection-dominated accretion flows. They found that for $\beta \sim 1$, i.e. approximately equipartition magnetic fields, the turbulence primarily heats the electrons.

For weaker magnetic fields, the protons are primarily heated. The division between electron and proton heating occurs between $5 < \beta < 100$, depending on unknown details of how Alfvén waves are converted into whistlers at the proton gyroscales.

The cascade of Alfvén waves, which are weakly damped down to the scale of the proton gyro-radius $k_\perp \rho_i \sim 1$ is a subject of gyro-kinetic models (see for a review Schekochihin et al. 2009). The models can be of interest for the parallel shock precursor heating assuming an efficient cascading of the CR-driven magnetic fluctuations down to the $k_\perp \rho_i \sim 1$ regime. The cascading still remains to be demonstrated since the CR-current driven modes are very different from the standard Alfvén waves. If the cascading occurs, then the continuity equation (1) can be reduced to the equation for $b_k^2(k_\perp) = k_\perp^2 \int dk_\parallel W(\mathbf{k})$ – the energy density of the anisotropic magnetic turbulence as a function of the perpendicular wavenumber (see, e.g., Howes 2010; Cranmer and van Ballegooijen 2012):

$$\frac{\partial b_k^2}{\partial t} + k_\perp \frac{\partial \epsilon(k_\perp)}{\partial k_\perp} = S(k_\perp) - \Gamma(k_\perp) b_k^2, \tag{9}$$

where the energy injection rate is S (non-zero only at the driving scale $k_\perp = k_0$), the linear energy damping rate is Γ, and $\epsilon(k_\perp)$ is the energy cascade rate. To specify the energy cascade rate both advection and diffusion in the wavenumber space models are used (see, e.g., Cranmer and van Ballegooijen (2012) for a recent discussion). Assuming critical balance at all scales and using the energy cascade rate in the form of the advection in the wavenumber space:

$$\epsilon(k_\perp) = C_1^{-3/2} k_\perp \overline{\omega} b_k^3$$

Howes (2010) obtained the steady state solution for the energy cascade rate as

$$\epsilon(k_\perp) = \epsilon_0 \exp\left\{ - \int_{k_0}^{k_\perp} C_1^{3/2} C_2 \frac{\overline{\Gamma}(k'_\perp)}{\overline{\omega}(k'_\perp)} \frac{dk'_\perp}{k'_\perp} \right\}, \tag{10}$$

where C_1 and C_2 are the dimensionless Kolmogorov constants ($C_1 = 1.96$ and $C_2 = 1.09$) and ϵ_0 is the rate of energy input at k_0. Howes (2010) used the normalized eigenfrequencies $\overline{\omega}(k_\perp)$ from the linear gyrokinetic dispersion relations and the damping rates $\overline{\Gamma}_s$ due to different plasma species from Howes et al. (2006) and Eq. (10) (where $s = i, e$), to calculate the spectrum of heating by species

$$Q_s(k_\perp) = C_1^{3/2} C_2 (\overline{\Gamma}_s / \overline{\omega}) \epsilon(k_\perp) / k_\perp .$$

The ion damping peaks at $k_\perp \rho_i \sim 1$, while the electron damping peaks at $k_\perp \rho_i \gg 1$ unless $T_i/T_e \lesssim m_e/m_i$. The energy that passes through the peak of the ion damping at $k_\perp \rho_i \sim 1$ would lead to electron heating assuming both the cascading and the damping times are shorter than the advection time through the shock precursor. Then the total (integrated over $k_\perp \rho_i \gtrsim 1$) ion-to-electron heating rate due to the kinetic dissipation of the turbulent cascade, $Q_i/Q_e(\beta_i, T_i/T_e)$ can be approximately fitted with

$$Q_i/Q_e = c_1 \frac{c_2^2 + \beta_i^p}{c_3^2 + \beta_i^p} \sqrt{\frac{m_i T_i}{m_e T_e}} e^{-1/\beta_i}, \tag{11}$$

where $c_1 = 0.92$, $c_2 = 1.6/(T_i/T_e)$, $c_3 = 18 + 5\log(T_i/T_e)$, and $p = 2 - 0.2\log(T_i/T_e)$. A slightly better fit for $T_i/T_e < 1$ occurs with the coefficients $c_2 = 1.2/(T_i/T_e)$ and $c_3 = 18$ (Howes 2010). The model is valid for the parameter range $0.01 \leq \beta_i \leq 100$ and

$0.2 \leq T_i/T_e \leq 100$. The heating rate Q_i/Q_e is an approximately monotonic function of β_i that is only weakly dependent of T_i/T_e.

The simplified model of the electron and ion heating discussed above assumed the nonlinear collisionless cascading from the energy containing scale of wavenumber $k_* R_g \sim 1$ where the amplitude of amplified magnetic field is δB_* that is determined by the gyroscale R_g of the energy containing accelerated particles to the thermal ion gyroscale $k_\perp \rho_i \sim 1$. In the shock frame the advection time of the incoming plasma through the CR precursor $\tau_{\rm adv} \sim \lambda_* \, c/v_{\rm sh}^2$. Therefore for efficient heating of the plasma species the cascading time τ_c must be shorter than $\tau_{\rm adv}$. If the cascading time is determined by the turn-over time of the energy containing magnetic "vortex" $\tau_c^{-1} \sim k_* \delta B_*/\sqrt{4\pi\rho}$ then the condition of efficient plasma heating in the shock precursor by the CR-driven turbulence can be written as

$$\frac{\tau_{\rm adv}}{\tau_c} = \eta \, \frac{c}{v_{\rm sh}^2} \, \frac{\delta B_*}{\sqrt{4\pi\rho}} > 1, \tag{12}$$

where $\eta = \lambda_*/R_g > 1$. The amplitude of amplified magnetic field likely scales with the shock velocity as $\delta B_* \propto v_{\rm sh}^{\rm b}$, where $1 \leq {\rm b} \leq 1.5$ (see, e.g., Vink 2012). The condition (12) predicts a less efficient plasma heating in the CR-precursor of the faster shocks.

Heat conduction that we did not discuss here may play a role in the electron temperature distribution in the shock precursor (c.f. Breech et al. 2009). The nonlinear dynamics of the the CR-driven magnetic fluctuations in the shock precursor deserves thorough modeling. Malkov et al. (2012) have obtained fully nonlinear exact solutions of the *ideal* 1D-MHD supported by the CR return current. The solutions occur as localized spikes of circularly polarized Alfvén envelopes (solitons or breathers). The sufficiently strong solitons in the model run ahead of the main shock and stand in the precursor, being supported by the return current. The CR-shock precursor in the model is dissipationless.

The electron and ion temperatures in the shock precursor determine the injection of particles into the CR acceleration regime. The temperatures can be tested by optical spectroscopy of supernova shocks. CR-modification of shocks with modest speed of a few hundred km s^{-1} may yield lower post-shock temperatures and thus make the post-shock flow switch to a radiative regime.

5 Spectroscopy of a CR-modified radiative shock [1]

Consider a one-dimensional flow around a collisionless shock consisting of three zones: a) the pre-shock, where the unperturbed interstellar matter is preionized and preheated by the radiation (and energetic particles) generated in the downstream and where strong fluctuations of magnetic field may be generated by the CR anisotropy, b) the thin shock front (a "viscous jump") where a substantial part of the kinetic energy of the bulk upstream flow is converted into energy of thermal motions, and c) the post-shock,

[1] This section uses some results of numerical code `SHELLS` currently developed by A.M. Bykov, A.E. Vladimirov, and A.M. Krassilchtchikov. This code is used to model the steady-state structure and broadband continuum and line emission spectra of radiative shocks. The model accounts for the impact of efficient CR acceleration on the shock compression ratio and the postshock flow. The code incorporates modern atomic data and allows us to consider in detail the non-equilibrium microscopic, thermodynamical and radiative processes that determine the plasma flow.

where the hot flow cools down, radiating continuum and line emission. We discuss here a class of shock flows in partly ionized media, the so-called *radiative shocks*, where the power radiated away from the post-shock flow is a sizeable fraction of the total kinetic and magnetic power dissipated at the shock (see, e.g., Spitzer 1978; Draine and McKee 1993).

Without a significant impact on accuracy, one may assume that the pre-shock is isothermal, and the flow is in a steady state (see also a comment about the equilibrium between the pre-shock ionization state and the ionizing flux at the end of Section 2) . However, the ionization state of the plasma is non-uniform: the ionization level increases toward the subshock, as the gas absorbs the ionizing radiation flux emerging from the hot downstream region. This photoionization does not have a significant impact on the thermal state of the gas, because the hot electrons produced by photoionization do not have sufficient time to collisionally equilibrate with the atoms and ions. CR particles may contribute to gas ionization and heating in the interstellar clouds and shells (e.g., Spitzer 1978; Bozhokin and Bykov 1994). The effect of CRs may be important in the vicinity of fast Balmer-type interstellar shocks as it has been demonstrated by Morlino et al. (2012a), who did not account for the photo processes, though. Radiative shocks are expected to occur in relatively dense environment and, therefore, have velocities typically well below 1,000 km s^{-1}. In such an environment, photo processes can provide a high ionization degree of the upstream gas for sufficiently high shock speeds. If CR acceleration is weak, the photoionization becomes significant for shock velocities above 100 km s^{-1}. However, if CR acceleration is efficient, the downstream temperature is reduced and the shock compression is increased, which means that strong photoionization in the precursor occurs at much greater shock speeds See Fig. 4 for an illustration of the effect of CR acceleration on precursor ionization. We demonstrate below the effect of the CR fluid on the shock compression and spectra of radiative shocks.

The jump conditions at the shock are either given by the Rankine-Hugoniot equations, or, if the shock structure is assumed to be modified by accelerated particles (e.g., Bykov 2004; Vladimirov et al. 2008, and references therein), the compression ratio can be parameterized by the fraction $Q_{\rm esc}$ of bulk flow energy carried away by these particles. The subshock is the standard gas viscous shock of a Mach number $\mathcal{M}_{\rm sub}$. For that simplified *two-fluid* model of a strong CR-modified shock the effective ion temperature in the downstream $T_{\rm i}^{(2)}$ can be estimated for a shock of a given velocity, if $r_{\rm tot}$ and $r_{\rm sub}$ are known:

$$T_{\rm i}^{(2)} \approx \phi(\mathcal{M}_{\rm sub}) \cdot \frac{\mu\ v_{\rm sh}^2}{\gamma_{\rm g} r_{\rm tot}^2(v_{\rm sh})}, \quad \text{where} \quad \phi(\mathcal{M}_{\rm sub}) = \frac{2\gamma_{\rm g}\mathcal{M}_{\rm sub}^2 - (\gamma_{\rm g}-1)}{(\gamma_{\rm g}-1)\mathcal{M}_{\rm sub}^2 + 2}. \qquad (13)$$

Single fluid strong shock heating represents the limit $\mathcal{M}_{\rm sub} = \mathcal{M}_{\rm s} \gg 1$, since there is no precursor in that case the temperature behind a strong shock is determined by the standard scaling

$$T^{(2)} \approx 2 \cdot \frac{(\gamma_{\rm g}-1)}{(\gamma_{\rm g}+1)^2}\ \mu v_{\rm sh}^2 = 1.38 \cdot 10^7\ v_{\rm s8}^2\ (K), \qquad (14)$$

In single-fluid systems the compression ratio $r_{\rm tot} = r_{\rm sub} \to (\gamma_{\rm g}+1)/(\gamma_{\rm g}-1)$ does not depend on the shock velocity and Eq.(13) reduces to Eq.(14). However, in multi-fluid shocks the total compression ratio depends on the shock velocity and could be substantially higher than that in the single-fluid case. Consequently, the post-shock

temperature in a multi-fluid shock is lower than the post-shock temperature in a single-fluid shock of the same speed. This allows us to determine the CR acceleration efficiency using observations of post-shock temperatures and shock speeds, or the entropy profiles in the accretion shocks of clusters of galaxies (Bykov 2005; Bykov et al. 2008; Brüggen et al. 2012; Fujita et al. 2013). It is convenient to introduce the scaling $r_{\rm tot}(v_{\rm sh}) \propto v_{\rm sh}^{\xi}$ to describe the different cases of strong shock heating (Bykov et al. 2008). Then from Eq. (13) $T_{\rm i}^{(2)} \propto \phi(\mathcal{M}_{\rm sub}) \cdot v_{\rm sh}^{2(1-\xi)}$. The subshock Mach number $\mathcal{M}_{\rm sub}$ depends, in general, on $\mathcal{M}_{\rm s}$ and $\mathcal{M}_{\rm a}$. Thus, the index σ approximates the velocity dependence of $\phi(\mathcal{M}_{\rm sub}) \propto v_{\rm sh}^{\sigma}$. Finally, if $T_{\rm i}^{(2)} \propto v_{\rm sh}^{a}$, then the index $a = 2(1-\xi)+\sigma$. For the case of shock precursor heating by CR generated Alfvén waves, the index $a \approx 1.25$ (Bykov 2005). The effects of neutrals due to charge exchange in the shock downstream with heated ions that results in a flux of high-velocity neutrals that return upstream were studied by Blasi et al. (2012) and Ohira (2012). They found that the return flux of neutrals may result in the reduced shock compression ratio and spectral steepening of test particles accelerated at the shocks slower than about 3000 km s^{-1}. The return flux of neutral atoms may also affect the radiation spectrum of the post-shock flow that we are modeling.

The ratio of the electron to ion temperature immediately after the subshock, $T_e/T_i = \delta_e$, is considered as a free parameter in our model. It can be estimated from observations as discussed in Section 3. It is varied in the range from $\sqrt{m_e/m_p} \approx 0.023$ to 1. Observations typically show low values of δ_e in shocks faster than 1000 km s^{-1}, and values closer to 1 in slower shocks (e.g., Ghavamian et al. 2001, 2007; Rakowski et al. 2008; Helder et al. 2010).

The post-shock plasma is treated as a stationary two-temperature single fluid flow consisting of ions, electrons, and neutral atoms that are ideal nonrelativistic gases. The neutral and ion temperatures may actually differ (Heng et al. 2007; van Adelsberg et al. 2008), but that is only important just behind a very fast shock in partially neutral gas, and it matters mainly for diagnostics based on the Hα line profile. For the considered here ranges of shock speeds and matter densities the temperature equilibration scales are below 10^{15} cm^{-2}, while the line emission zone typically lies well above 10^{16} cm^{-2} downstream.

Let z and μ be the average charge and mass of an ion, $\zeta \equiv m_e/\mu$ – the average electron to ion mass ratio. Then

$$\begin{aligned} n_e = z n_i,\ \rho_e = m_e n_e = z m_e n_i, \qquad (15)\\ \rho_i = \mu n_i,\\ \rho = n_i(z m_e + \mu) = n_i \mu (z\zeta + 1) \equiv n_i \mu / M(z),\\ M(z) = 1/(z\zeta + 1). \end{aligned}$$

Let ρ_0, v_0, and B_0 be the values of density, velocity, and frozen-in transverse magnetic field just before the shock, and v_a, T_i^a be the values of flow velocity and ion temperature in the immediate post-shock defined by jump conditions.

Then, the flow evolution downstream can be described by the following system of equations.

$$\rho v = \text{const} = \rho_0 v_0, \qquad (16)$$

$$\rho v^2 + p_e + p_i + p_m + p_{CR} = \text{const} \equiv \Pi \rho_0 v_0^2, \qquad (17)$$

$$\frac{3}{2}n_i v\frac{dT_i}{dx} = -n_i T_i\frac{dv}{dx} - \frac{3m_e}{\mu}\frac{n_e}{\tau_{ei}}(T_i - T_e), \tag{18}$$

$$\frac{3}{2}n_e v\frac{dT_e}{dx} = -n_e T_e\frac{dv}{dx} + \frac{3m_e}{\mu}\frac{n_e}{\tau_{ei}}(T_i - T_e) - \Lambda - \frac{3}{2}n_i T_e v\frac{dz}{dx}, \tag{19}$$

where $p_e + p_i = n_i k_B(zT_e + T_i) = \rho k_B M(zT_e + T_i)/\mu$, the magnetic pressure $p_m = B_0^2\rho^2/(8\pi\rho_0^2)$, $\Pi = v_a/v_0 + B_0^2/(8\pi\rho_0 v_0 v_a) + k_B M T_i^a(z\delta_e+1)/(v_0 v_a \mu) + Q_{\rm esc}/2$, $p_{CR} = (Q_{\rm esc}/2)\cdot\rho_0 v_0^2(v_a/v)^{4/3}$, Λ is the cooling function, τ_{ei} is the electron-ion equilibration time, and the last term of equation (19) denotes electron cooling due to ionization.

The cooling term Λ is calculated as

$$\Lambda = n^2\Lambda_{coll} + n_e\sum_{i,j}(n_{i,j}\alpha_{i,j}E_{i,j}^{rec} + n_{i,j}C_{i,j}h\nu_j) - \tag{20}$$
$$-4\pi\sum_{i,j}\int_{\nu_j}^{\infty} d\nu\cdot\sigma_{i,j}^{ph}(1-\nu_j/\nu)n_{i,j}J_\nu,$$

where i denotes the chemical element and j denotes the ionization state of an ion (j=0 corresponds to a neutral atom). Here Λ_{coll} is due to electron-ion collisions including electron bremsstrahlung and line emission of the ions excited by electron impact, though it does not include emission due to radiative recombination; $\alpha_{i,j}$ is the recombination rate $\{j+1\}\to\{j\}$; $E_{i,j}^{rec}$ is the average energy on the recombining electrons; $C_{i,j}$ is the rate of collisional ionization; $\sigma_{i,j}^{ph}$ is the photoionization crossection of the ion state j; J_ν is the angle-averaged density of ionizing radiation at frequency ν:

$$J_\nu(x) = \frac{1}{4\pi}\int_{-1}^{1} 2\pi\ I_\nu(\mu,x)\ d\mu. \tag{21}$$

where $\mu = cos(\theta)$, θ is the angle between the normal to the shock front and the direction of emitted photons.

The evolution of the ionization state j of an ion i in the downstream flow is determined as

$$v\frac{dn_{i,j}}{dx} = n_e\left(n_{i,j-1}\tilde{C}_{i,j-1} - n_{i,j}\tilde{C}_{i,j} - n_{i,j}\tilde{\alpha}_{i,j} + n_{i,j+1}\tilde{\alpha}_{i,j+1}\right) + \tag{22}$$
$$+n_{i,j-1}R_{i,j-1} - n_{i,j}R_{i,j} +$$
$$+\sum_{s=H,He,He^+} n_s\left[n_{i,j-1}V_{s,i,j-1}^{ion} - n_{i,j}(V_{s,i,j}^{ion} + V_{s,i,j}^{rec}) + n_{i,j+1}V_{s,i,j+1}^{rec}\right],$$

where $R_{i,j}$ is the photoionization rate, V_s^{ion} and V_s^{ion} are the rates of ionization and recombination via charge exchange reactions with the ion s, $\tilde{C}_{i,j} = C_{i,j} + C_{i,j}^{\rm auto}$, where $C_{i,j}^{\rm auto}$ is the autoionization rate, $\tilde{\alpha}_{i,j} = \alpha_{i,j} + \alpha_{i,j}^{2e}$, where $\alpha_{i,j}^{2e}$ is the dielectronic recombination rate.

To obtain the ionizing radiation field a transfer equation can be solved both in the downstream and in the upstream:

$$\cos\theta\cdot\frac{dI_\nu}{dx} = j_\nu - \kappa_\nu I_\nu, \tag{23}$$

where θ is the angle between the normal to the shock front and the direction of emitted photons. In this equation, the absorption coefficient $\kappa_\nu = \sum_{i,j} n_{i,j}\sigma_{i,j}^{ph}$ is determined by bound-free transitions in all ion species. The ionizing emission is generated as a)

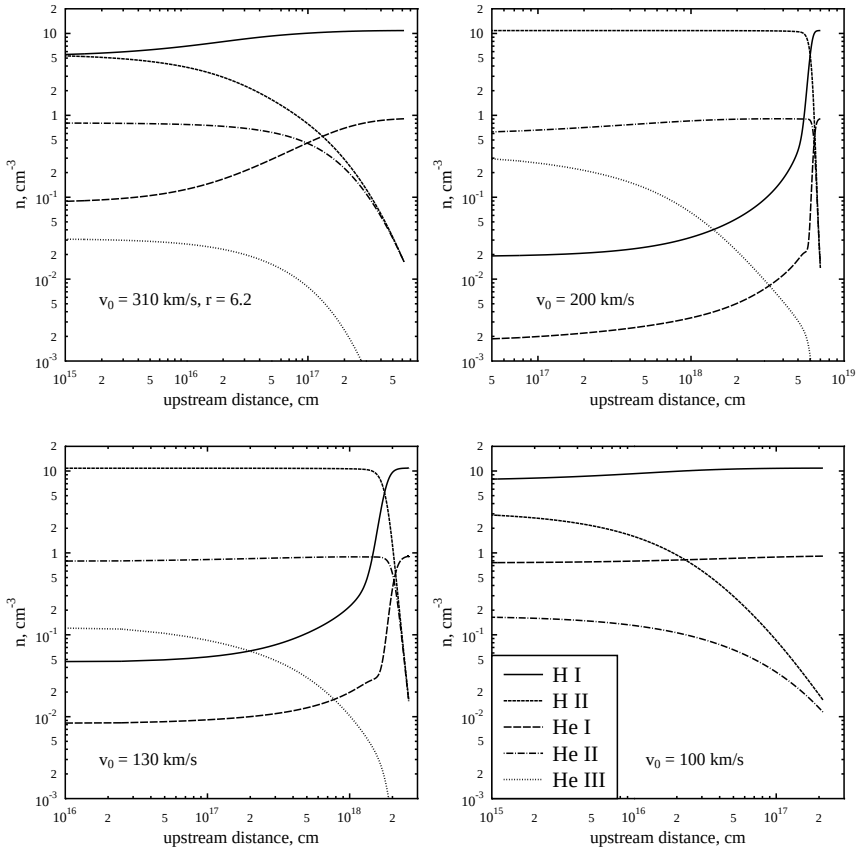

Fig. 4 Hydrogen and helium pre-shock (photo)ionization in the shock upstream for four sets of shock parameters simulated with the model of radiative shock accounting for the effect of CR escape on the shock compression r (the CR-modified case is shown in the top left panel). Within the presented model $r = 6.2$ corresponds to 30% of the flow energy being converted into CRs.

permitted ultraviolet and optical lines excited by an electronic impact, b) recombination line cascades of hydrogen and helium, c) free-free continuum of electrons scattering at ions, d) 2-photon continuum emission of H- and He-like ions where metastable levels are collisionaly populated, e) recombination continuum emission.

The relative contribution of each of the mechanisms to the ionizing photon field is illustrated in Figure 5. The dominating 2-photon continuum emission comes mainly from He I and He II and the dominating ultraviolet line emission comes mainly from He I, He II, and oxygen ions upto O V. It should be noted that in the presented model the electron temperatures just after the shock are assumed to be low ($\delta_e \sim 10^{-2}$) and equilibrate with the ion temperatures downstream via Coulomb collisions.

All the ionizing lines except Lyα were considered optically thin. The optically thick case of Lyα was treated according to the standard 2-level formalism adopted from Mihalas and Mihalas (1984).

line	λ	r = 4.6	r = 5.3	r = 6.2	line	λ	r = 4.6	r = 5.3	r = 6.2
He II	304 Å	2640	750	1.1	[S II]	6718 Å	67.1	27.8	16.1
O IV	554 Å	201	14.7	···	[S II]	6733 Å	43.9	18.9	10.6
He I	584 Å	72.5	212	103	[Fe II]	1.28 μm	126	85.1	51.1
O V	630 Å	24.5	···	···	[Fe II]	1.62 μm	29.0	19.4	11.6
O III	833 Å	98.4	142	0.5	[Fe II]	5.30 μm	95.2	78.2	49.4
C III	977 Å	637	770	52.1	[S IV]	10.51 μm	2.1	2.0	0.1
O VI	1034 Å	···	···	···	[Ne II]	12.81 μm	40.3	26.6	8.1
Lyα	1216 Å	5500	10000	17000	[Ne III]	15.55 μm	29.7	12.6	···
N V	1240 Å	2.9	0.1	···	[Fe II]	17.94 μm	10.1	8.1	5.1
Si IV	1397 Å	114	122	2.1	[S III]	18.71 μm	1.3	1.8	1.1
C IV	1549 Å	858	190	0.1	[Fe II]	24.52 μm	1.8	1.4	0.9
He II	1640 Å	58.5	12.6	···	[O IV]	25.91 μm	12.4	2.9	···
C III]	1908 Å	219	290	50.9	[Fe II]	26.00 μm	47.5	43.5	29.6
[O II]	3729 Å	236	221	289	[S III]	33.50 μm	1.7	2.4	1.6
[Ne III]	3870 Å	23.6	14.9	···	[Si II]	34.82 μm	218	122	51.8
[Ne III]	3969 Å	7.1	4.5	···	[Fe II]	35.35 μm	10.2	9.2	6.2
He II	4687 Å	6.2	1.1	···	[Ne III]	36.02 μm	2.6	1.1	···
Hβ	4861 Å	100	100	100	[N III]	57.34 μm	1.7	1.6	0.1
[O III]	4960 Å	48.3	49.0	0.4	[O I]	63.19 μm	28.7	12.7	4.9
[O III]	5008 Å	144	146	1.0	[O III]	88.36 μm	9.8	8.2	0.1
[O I]	6300 Å	27.4	7.0	3.1	[N II]	121.8 μm	6.2	3.8	2.0
[O I]	6363 Å	27.3	6.9	3.1	[O I]	145.5 μm	3.8	1.9	0.8
Hα	6565 Å	302	310	321	[C II]	157.7 μm	18.3	13.5	7.9
[N II]	6550 Å	46.6	24.6	19.9	Hβ	4863 Å	6.38	5.61	5.05
[N II]	6585 Å	142	75.1	60.7					

Table 1 Model line strengths in percent of Hβ flux for $v_0 = 200$ km/s at CR-modified compression ratios $r = 4.6$, 5.3, 6.2. The last line presents absolute flux in Hβ 4861 Åline in 10^{-6} erg cm^{-2} s^{-1} sr^{-1} polariz^{-1} .

He II	304 Å	2600	[N II]	6585 Å	139
O IV	554 Å	597	[S II]	6718 Å	71.6
He I	584 Å	45.1	[S II]	6733 Å	45.1
O V	630 Å	509	[Fe II]	1.28 μm	288
O III	833 Å	179	[Fe II]	1.62 μm	69.4
C III	977 Å	438	[Fe II]	5.30 μm	204
O VI	1034 Å	0.6	[S IV]	10.51 μm	2.3
Lyα	1216 Å	641	[Ne II]	12.81 μm	61.2
N V	1240 Å	14.3	[Ne III]	15.55 μm	24.4
Si IV	1397 Å	138	[Fe II]	17.94 μm	36.4
C IV	1549 Å	1080	[S III]	18.71 μm	1.9
He II	1640 Å	74.9	[Fe II]	24.52 μm	6.7
C III]	1908 Å	152	[O IV]	25.91 μm	15.0
[O II]	3729 Å	254	[Fe II]	26.00 μm	114
[Ne III]	3870 Å	23.6	[S III]	33.50 μm	1.8
[Ne III]	3969 Å	7.1	[Si II]	34.82 μm	143
He II	4687 Å	8.9	[Fe II]	35.35 μm	25.2
Hβ	4861 Å	100	[Ne III]	36.02 μm	2.1
[O III]	4960 Å	52.2	[N III]	57.34 μm	1.0
[O III]	5008 Å	156	[O I]	63.19 μm	47.4
[O I]	6300 Å	35.7	[O III]	88.36 μm	4.0
[O I]	6363 Å	35.5	[N II]	121.8 μm	1.9
Hα	6565 Å	302	[O I]	145.5 μm	5.6
[N II]	6550 Å	45.5	[C II]	157.7 μm	7.3

Table 2 Model line intensities expressed in percent of the 4861 Å Hβ line instensity, which amounts here to 7.87×10^{-6} erg cm^{-2} s^{-1} sr^{-1} polariz^{-1} .

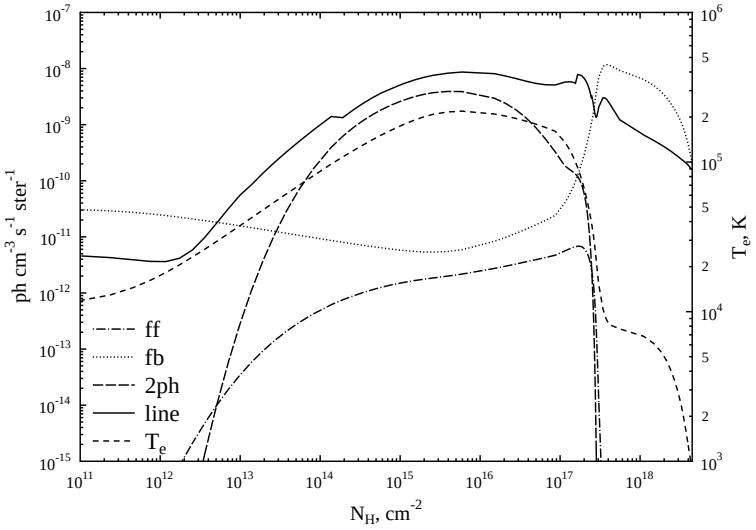

Fig. 5 Production rate of ionizing photons ($h\nu > 1$ Ry) in the downstream of a 130 km/s shock penetrating into a 10 cm^{-3} medium of solar abundance. Here "fb" denotes recombination continuum emission, "ff" denotes free-free continuum of electrons scattering at ions, "2ph" stands for 2-photon continuum emission of H- and He-like ions, and "line" denotes permitted ultraviolet lines excited by an electronic impact. The dashed line illustrates the simulated electron temperature profile in the downstream. The photons produced in the optically thin part of the downstream are ionizing the upstream flow.

Figures 4 through 8 and Tables 1 and 2 demonstrate the results of modeling with SHELLS. The impact of efficient CR acceleration on the shock is accounted for in all calculations by using a reduced downstream temperature and the CR pressure in the shock downstream.

The steady-state pre-shock ionization structure is shown in Figure 4 for shocks with speeds of 100, 130, 200, and 310 km s^{-1} illustrating also an effect of the CR fluid on the pre-shock ionization. The plasma temperature and gas compression just behind the CR modified shock affect the ionization structure. One can see in Figure 4 that the ionization structure of 310 km s^{-1} shock modified by CRs may be similar to that of 100 km s^{-1} shock without CRs fluid effect. This Figure shows the ionization level of hydrogen and helium; however, all abundant chemical species up to Fe are tracked in the calculation. At speeds of approximately 130 km/s and above, hydrogen upstream becomes completely ionized, and the extent of the radiative precursor is determined by the competition between hydrogen and helium recombination and photoionization.

Figure 6 illustrates the downstream cooling region of a 200 km/s shock. Three lines correspond to three models with different assumptions regarding the efficiency of CR acceleration. For efficient acceleration, energy conservation requires greater compression ratio and lower downstream temperature. The three cases shown here illustrate shocks with compression ratios of 4.6, 5.3 and 6.2.

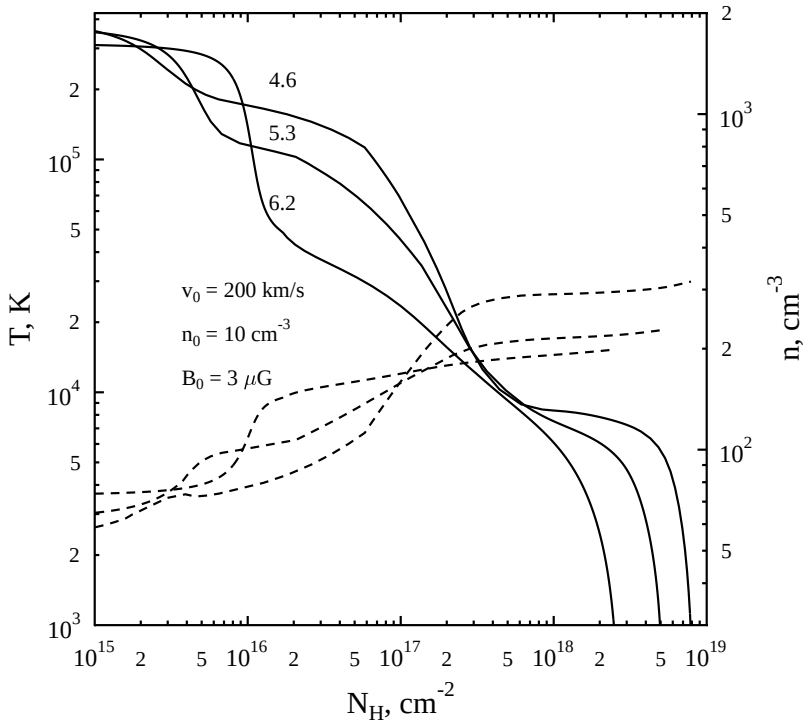

Fig. 6 Gas temperature (solid lines) and density (dotted lines) in the downstream cooling region of three 200 km/s shocks. Three lines correspond to three models with different assumptions regarding the efficiency of CR acceleration. Within the presented model $r = 6.2$ corresponds to $Q_{\rm esc} = 30\%$ of the flow energy being converted into CRs, $r = 5.3$ corresponds to $Q_{\rm esc} = 20\%$, and $r = 4.6$ corresponds to $Q_{\rm esc} = 10\%$.

Shown in Figure 7 is the result of a calculation with shock and ISM parameters plausible for the region of interaction of the north-eastern shell of the SNR IC 443 with an interstellar cloud. Unperturbed gas density is $n_0 = 15$ cm^{-3}, shock velocity $v_0 = 130$ km/s, and perpendicular magnetic field $B_0 = 3$ μG are assumed. The temperature and total density of the plasma are plotted as a function of gas column density from the subshock. These quantities are then used to calculate the radiative transfer of emission lines in the cooling flow, which can be used for shock diagnostics. Figure 8 shows the profiles of two of the most prominent infrared lines (with respect to estimated backgrounds) for this case: C II 157.7 μm and N II 205.3 μm.

The model presented in this Section may be used to diagnose various parameters of radiative shocks with observed infrared lines, including the cosmic ray acceleration efficiency.

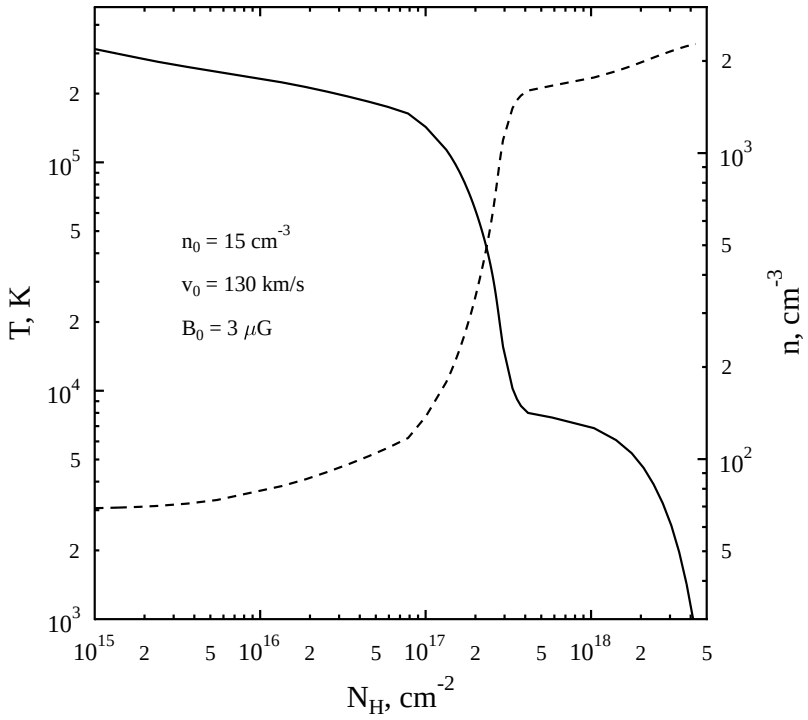

Fig. 7 Post-shock flow profile for shock and ISM parameters plausible for the region of interaction of the north-eastern shell of IC 443 SNR with an interstellar cloud. Here the upstream density $n_0 = 15$ cm^{-3}, the shock velocity $v_0 = 130$ km/s, and the perpendicular magnetic field $B_0 = 3$ μG.

6 Formation of CR spectral breaks in partly ionized shock precursors

6.1 Gamma-ray observations

The neutral component of the interstellar medium may manifest itself in the gamma-ray emission of some collisionless shocks.

The recent Fermi-LAT observations of the so-called molecular SNRs W44 and IC 443 (Abdo et al. 2010a,2010b; Ackermann et al. 2013) indicate that the spectra of the gamma-ray producing protons (integrated over the emission region) are typically steeper than the DSA predictions for the spectra of the CRs confined in the acceleration region. The steep photon spectra has been found in the high energy gamma-ray spectra of some other remnants measured by, e.g., the CANGAROO (Enomoto et al. 2002), H.E.S.S (Aharonian et al. 2006) and MAGIC (Carmona 2011) atmospheric Cherenkov telescopes.

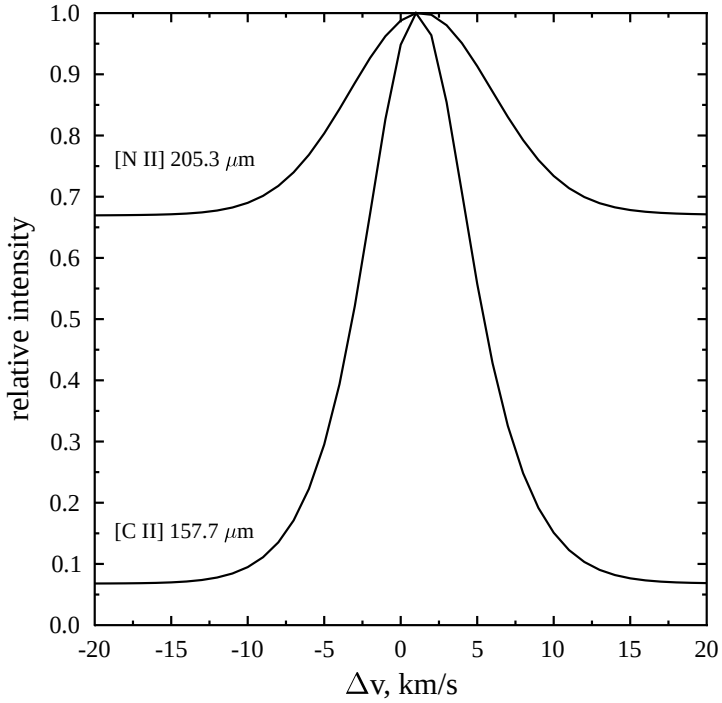

Fig. 8 [C II] 157.7 μm and [N II] 205.3 μm line profiles for the backgrounds of 140 MJy/sr and 130 MJy/sr, respectively, estimated for the north-eastern shell of IC 443 SNR with Herschel Spot (for the date 22/09/2010).

Particles accelerated by DSA mechanism generally comprised two distinct populations – CRs confined in the accelerator and the CRs escaping the system and these two populations have very different spectral shapes. The observed gamma-ray emission is a sum of the two contributions (see, e.g., Ellison and Bykov 2011). The common feature of the molecular SNRs is a significant amount of dense molecular gas in their surroundings. It has been argued on this ground (Malkov et al. 2005), that when a SNR interacts with a dense molecular cloud complex, the conditions for particle confinement to the shock are different from those adopted in conventional DSA modeling. Since the propagation of resonant Alfvén waves is inhibited by ion-neutral collisions, some particles are not confined and so escape the emission volume (e.g. Drury et al. 1996; Bykov et al. 2000; Malkov et al. 2005). The accelerated particle partial escape should result in a spectral break in their spectrum and thus, in that of the observed gamma emission. In a clear-cut case of such a limited CR confinement, the spectral index at the break should change by exactly one power $\Delta q = 1$ due to an effective reduction of the particle momentum space dimensionality by one, since particles are

confined in coordinate space only when they are within a slab in momentum space oriented perpendicular to the local magnetic field.

The most convincing evidence for the breaks of index one are the recent Fermi-LAT and AGILE observations of W44 (Abdo et al. 2010a; Uchiyama et al. 2010; Giuliani et al. 2011) (re-analyzed in (Malkov et al. 2011)) and MAGIC observations of the SNR W51C (Carmona 2011; Aleksić et al. 2012) These observations are encouraging in that they unambiguously confirm the breaks. They demonstrate departure from the traditional DSA models in fully ionized plasma where the proton spectrum is a single power law with an exponential cutoff. A possible explanation to the spectral break in the gamma-ray emission of these objects is that neutral atoms modify the nature of wave-particle interactions, leading to a spectral break. This idea is discussed below.

6.2 The DSA mechanism

A great deal of the success of the diffusive shock acceleration mechanism (DSA) is due to its ability to reproduce the observed power law spectra associated with possible CR accelerators, such as SNR shocks. For a classical step-like shock, propagating into an ionized medium that supports sufficient CR scattering on both sides of the shock, the mechanism predicts an almost universal power-law energy spectrum for the accelerated CRs, $\propto E^{-q}$, with an index $q = (r+2)/(r-1)$. It thus depends only on the shock compression r, that is, however, close to four for strong shocks. The backreaction of the accelerated CRs on the shock structure may change this result noticeably, but not dramatically. For strong shocks, $\mathcal{M} \gg 1$, the spectrum hardens from $q = 2$ to $q \simeq 1.5$, at most. This change is largely due to an enhanced compression of the shock that results from the CR escape flux and the reduction of the adiabatic index of the CR/thermal-plasma mixture compared to the ordinary plasma (i.e., $\gamma = 5/3 \to 4/3$). More problematic is to soften the CR spectrum by their backreaction effects on the shock environment. This is intuitively understandable, since spectrum steepening should diminish the backreaction coming from the softening of the equation of state ($\gamma \to 4/3$) and, especially, from the CR escape flux.

The recent Fermi-LAT observations of the SNRs W44 and IC 443 (Abdo et al. 2010a,2010b) also urge a second look at the DSA mechanism (see Section 6.1).

6.3 Mechanism for a spectral break

When a SNR shock approaches a molecular cloud (MC) or a pre-supernova swept-up shell with a significant amount of neutrals, confinement of accelerated particles deteriorates. Due to the particle interaction with magnetic fluctuations, confinement requires their scales to be similar to the particle gyroradii (Drury 1983; Blandford and Eichler 1987). However, strong ion-neutral collisions make the wave-particle interactions more sensitive to the particle pitch angle, which can be understood from the following consideration.

While the waves are in a strongly ionized (e.g., closer to the shock) medium they propagate freely in a broad frequency range at the Alfvén speed $V_A = B/\sqrt{4\pi\rho_i}$ with the frequencies $\omega = kV_A$. Here k is the wave number (assumed parallel to the local field $\mathbf{B}$) and ρ_i is the ion mass density. As long as the Alfvén wave frequency is higher than the ion-neutral collision frequency ν_{in}, the waves are only weakly damped. When,

on the other hand, the ion-neutral collision frequency is higher (deeper into the cloud), neutrals are entrained by the oscillating plasma and the Alfvén waves are also able to propagate, albeit with a factor $\sqrt{\rho_i/\rho_0} < 1$ lower speed, where ρ_0 is the neutral density. The propagation speed reduction occurs because every ion is now "loaded" with ρ_0/ρ_i neutrals. Now, between these two regimes Alfvén waves are heavily damped and even disappear altogether for sufficiently small $\rho_i/\rho_0 \ll 0.1$. The evanescence wave number range is then bounded by $k_1 = \nu_{in}/2V_A$ and $k_2 = 2\sqrt{\rho_i/\rho_0}\nu_{in}/V_A$. These phenomena have been studied in detail in (Kulsrud and Pearce 1969; Zweibel and Shull 1982), and specifically in the context of the DSA in (Völk et al. 1981; Drury et al. 1996; Bykov et al. 2000; Reville et al. 2008). Now we turn to their impact on the particle confinement and emissivity.

In the framework of a quasilinear wave-particle interaction, the wave number k is approximately related to the parallel (to the magnetic field) component of the particle momentum $p_\parallel$ by the cyclotron resonance condition $kp_\parallel/m = \pm\omega_c$, where the (non-relativistic) gyro-frequency $\omega_c = eB/mc$. Note that the appearance of $p_\parallel = p\mu$, where μ is the cosine of the pitch angle instead of the often used "sharpened" (Skilling 1975) resonance condition $kp/m = \pm\omega_c$ is absolutely critical for the break mechanism. The frequency range where the waves cannot propagate may be conveniently translated into the parallel momentum range

$$p_1 < \left|p_\parallel\right| < p_2, \tag{24}$$

with

$$p_1 = 2V_A m\omega_c/\nu_{in}, \;\; p_2 = \frac{p_1}{4}\sqrt{\rho_0/\rho_i} > p_1. \tag{25}$$

That a spectral break must form at the photon energy corresponding to the particle momentum $p = p_1 = p_{br}$, can be readily explained as follows. The 'dead zones' $p_1 < \left|p_\parallel\right| < p_2$ imply that particles with $\left|p_\parallel\right| > p_1$ do not turn around (while moving along the magnetic field) and escape from the region of CR-dense gas collisions at a $p_\parallel/p$ fraction of the speed of light. More specifically, particles with $p_1 < \left|p_\parallel\right| < p_2$ escape because they are not scattered, whereas particles with $\left|p_\parallel\right| > p_2$, because they maintain the sign of $p_\parallel$, even though they scatter but cannot jump over the gap $p_1 < \left|p_\parallel\right| < p_2$. An exception to this rule are particles with sufficiently large $p_\perp$ that can be mirrored across the gap or overcome it via the resonance broadening.

The break can also be explained in terms of the confinement times of different groups of particles introduced above if we assume a low density pre-shock medium with clumps of dense, partially neutral, gas. Particles with $\left|p_\parallel\right| > p_1$ spend only short time $\tau_{\rm esc} \sim L_{\rm c}/c$ (where $L_{\rm c}$ is the size of the clump) inside the gas clumps. They propagate ballistically and their scattering time is assumed to be infinite, as there are no waves they can interact with resonantly ($p_1 < \left|p_\parallel\right| < p_2$) or they cannot change their propagation direction ($\left|p_\parallel\right| > p_2$). Particles with $\left|p_\parallel\right| < p_1$ are, on the contrary, scattered intensively in pitch angle, they frequently change their direction, and so sit in the clump for $\tau_{\rm conf} \sim L_{\rm c}^2/\kappa \sim L_{\rm c}^2/c^2\tau_{\rm sc}$. Here $\tau_{\rm sc}$ is their pitch-angle scattering time and κ is the associated diffusion coefficient. Not only $\tau_{\rm conf} \gg \tau_{\rm esc}$ is required, i.e., $\tau_{\rm sc} \ll L_{\rm c}/c$, but also $\tau_{\rm conf} > L_{\rm c}/U_{\rm sh}$, which means that the shock precursor is shorter than the clump $\kappa/U_{\rm sh} \lesssim L_{\rm CR} < L_{\rm c}$ (here $U_{\rm sh}$ is the shock velocity, and $L_{\rm CR}$ is the thickness of the CR front near the shock). The last condition ensures that particles with $p_\parallel > p_1$ that escape through the clump after having entered it from the shock

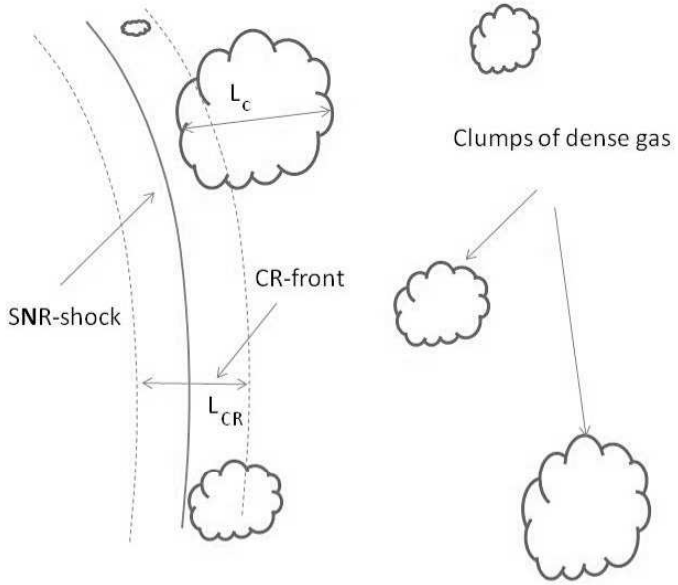

Fig. 9 SNR shock propagating into dense gas environment. The filling factor of the gas clumps is small, while some of them may be larger than the thickness of the CR layer near the shock front.

side, will not interact with the shock after they exit through the opposite side of the clump, thus escaping upstream, Fig.9. The reason for that is a low level of Alfvén wave turbulence ahead of the CR precursor. We also assume that the ambient magnetic field does not deviate strongly from the shock normal, in order to allow these particles to escape through the far side of the clump.

While particles with $p > p_1$ escape from the regions of enhanced gamma radiation (high gas density), an initially isotropic distribution of accelerated particles is maintained only in a slab in momentum space $\left|p_{\|}\right| < p_1$ and becomes thus highly anisotropic (a 'pancake' distribution). What matters for the integral emission, however, is a locally isotropic component $\overline{f}$ of this new proton distribution. It can be introduced by re-averaging the 'pancake' ($\left|p_{\|}\right| < p_1$) distribution in pitch angle, $\overline{f}\,(p) \equiv \int_0^1 f\,(p,\mu)\,d\mu$, and is readily obtained assuming that particles remaining in the dense gas (those with $\left|p_{\|}\right| < p_1$) maintain the flat pitch-angle distribution, i.e.

$$\overline{f}\,(p) = \int\limits_0^{\mu_1} f_0\,(p)\,d\mu = \begin{cases} (p_1/p)\,f_0\,(p)\,, & p \geq p_1 \\ f_0\,(p)\,, & p < p_1 \end{cases} \tag{26}$$

where $f_0(p)$ is the initial (isotropic) distribution function and $\mu_1 = \min\{p_1/p, 1\}$. Thus, the slope of the particle momentum distribution becomes steeper by exactly one power above $p = p_1 \equiv p_{\rm br}$. In particular, any power-law distribution $\propto p^{-q}$, upon entering an MC, turns into p^{-q-1} at $p \geq p_{\rm br}$, and preserves its form at $p < p_{\rm br}$.

Note that the broken power-law spectrum can only be maintained if the filling factor $f_{\rm gas}$ of the dense gas with the significant wave evanescence interval (p_1, p_2) is relatively small, $f_{\rm gas} \ll 1$, so that the overall particle confinement and thus the acceleration are not strongly affected. If, on the contrary, $f_{\rm gas} \sim 1$, the resonant particles would leak into the (p_1, p_2) gap and escape from the accelerator in large amounts, thus suppressing the acceleration. Note that particles with sufficiently high momenta $p > p_2 B_0/\delta B$, where $\delta B/B_0$ is the effective mirror ratio of magnetic perturbations, can "jump" over the gap. The primary p^{-q} slope should then be restored for such particles. Recent MAGIC observations of the SNR W51C (Carmona 2011; Aleksić et al. 2012) indeed point at such spectrum recovery at higher energies. It should also be noted, that the $\Delta q = 1$ break index is a limiting case of identical gas clumps. The integrated emission from an ensemble of clumps with different p_1 and p_2 should result in a more complex spectrum.

6.4 Break momentum

While the one power spectral break in the pitch-angle averaged particle distribution seems to be a robust environmental signature of a weakly ionized medium into which the accelerated particles propagate, the break momentum remains uncertain. According to eq.(25), p_{br} ($\equiv p_1$) depends on the magnetic field strength and ion density as well as on the ion-neutral collision rate $\nu_{in} = n_0 \langle \sigma V \rangle$. Here $\langle \sigma V \rangle$ is the product of the collision cross-section and collision velocity averaged over the thermal distribution. Using an approximation of (Draine and McKee 1993; Drury et al. 1996) for $\langle \sigma V \rangle$, p_{br} can be estimated as

$$p_{br}/mc \simeq 10 B_\mu^2 T_4^{-0.4} n_0^{-1} n_i^{-1/2}. \quad (27)$$

Here the gas temperature T_4 is measured in the units of $10^4 K$, magnetic field B_μ -in microgauss, n_0 and n_i (number densities corresponding to the neutral/ion mass densities ρ_0 and ρ_i) -in cm^{-3}. Note that the numerical coefficient in the last expression may vary depending on the average ion and neutral masses and can be higher by a factor of a few (Kulsrud and Pearce 1969; Nakano 1984) than the estimate in eq.(27) suggests. The remaining quantities in the last formula are also known too poorly to make an accurate independent prediction of the position of the break in the gamma ray emission region. Those are the regions near the blast wave where complicated physical processes unfold, as discussed earlier (Shull and McKee 1979; Draine and McKee 1993; Bykov et al. 2000). Also important may be the ionization by the low energy CRs accelerated at the blast wave. However, as their diffusion length is shorter than that of the particles with $p \gtrsim p_{br}$, we may assume that they do not reach the MC. Pre-ionization by the UV photons can also be ignored for the column density $N > 10^{19} cm^{-2}$ ahead of the shock beyond which they are absorbed (Uchiyama et al. 2010). Uchiyama et al. (2010), using the earlier data from (Reach et al. 2005) have also analyzed the parameters involved in eq.(27) and found the above estimate of p_{br} to be in a good agreement with the spectral break position measured by the Fermi-LAT. Nevertheless, we may run the argument in reverse and use the Fermi observations (Abdo et al. 2010a) of the gamma-ray spectrum of SNR W44 to determine the break momentum in the parent

particle spectrum and constrain the parameters in eq.(27). Since we also know the amount of the slope variation Δq, we can calculate the full spectrum up to the cut-off energy.

It should also be noted that in reality the break at $p = p_{\rm br}$ is not infinitely sharp for the following reasons. The break momentum may change in space due to variations of the gas parameters (eq.[27]), the resonance broadening (Dupree 1966; Achterberg 1981) near $p = p_1 = p_{\rm br}$ (so that particles with $p \sim p_1$ are still scattered, albeit weakly) and other factors, such as the contribution of small gas clumps with $L_c \ll L_{\rm CR}$, Fig.9. The small clumps are submerged in the CR front and the CRs that escape from them are readily replenished. Note that this effect may decrease the break index Δq. However, the conversion of the parent proton spectrum into the observable gamma emission introduces a significant smoothing of the break, so that even a sharply broken proton spectrum produces a smooth gamma spectrum. It provides an excellent fit to the Fermi gamma-ray data without an ad hoc proton break smoothing adopted by the Fermi-team (Abdo et al. 2010a) to fit the data.

7 Particle and gamma-photon spectra in molecular cloud SNRs

To calculate the particle spectra, we need to determine the degree of nonlinear modification of the shock structure. In principle, it can be calculated consistently, given the shock parameters and the particle maximum momentum, p_{max}. In the case of a broken spectrum, p_{br} likely plays the role of p_{max}, as a momentum where the dominant contribution to the pressure of accelerated particles comes from, thus setting the scale of the modified shock precursor. Note that in the conventional nonlinear (NL) acceleration theory, the cut-off momentum p_{max} plays this role, because the nonlinear spectra are sufficiently flat so as to make the pressure diverge with momentum, unlike the broken spectra.

One of the best documented gamma emission spectra comes from the SNR W44, so we fit these data using the above mechanism of the spectral break. The break in the photon spectrum is observed at about 2 GeV, which places the break in the proton distribution at about $p_{br} \simeq 7GeV/c$ (Abdo et al. 2010a). For the strength of the break $\Delta q = 1$, the spectrum above it is clearly pressure converging, so that the shock structure and the spectrum may be calculated using this break momentum as the point of the maximum in the CR partial pressure. More specifically, once the break momentum is set, one can use an analytic approach (Malkov and Drury 2001) for a stationary nonlinear acceleration problem using p_{br} as an input parameter.

Apart from p_{br}, the nonlinear solution depends on a number of other parameters, such as the injection rate of thermal particles into acceleration, Mach number, the precursor heating rate and the shock velocity V_s. Of these parameters the latter is known reasonably well, $V_s \approx 300$ km/s, the injection rate can be either calculated analytically for the parallel shock geometry (Malkov and Drury 2001), or inferred from the simulations (Gargaté and Spitkovsky 2012), while the other parameters are still difficult to ascertain. Fortunately, in sufficiently strong shocks the solution either stays close to the test particle (TP) solution (leaving the shock structure only weakly modified) or else it transitions to a strongly modified NL-solution regime. The TP regime typically establishes in cases of moderate Mach numbers, low injection rates and low p_{max} (now probably closer to p_{br}), while the NL regime is unavoidable in the opposite part of the parameter space.

In the TP regime the spectrum is close to a power-law with the spectral index 2 throughout the supra-thermal energy range. In the NL regime, however, the spectrum develops a concave form, starting from a softer spectrum at the injection energy, with the index $q \simeq (r_s + 2)/(r_s - 1) > 2$, where $r_s < 4$ is the sub-shock compression ratio. Then it hardens, primarily in the region $p \sim mc$, where both the partial pressure and diffusivity of protons change their momentum dependence. The slope reaches its minimum at the cut-off (break) energy, which, depending on the degree of nonlinearity, can be as low as 1.5 or even somewhat lower if the cut-off is abrupt. The question now is into which of these two categories the W44 spectrum falls? Generally, in cases of low maximum (or, equivalently, low spectral break $p_{br} \lesssim 10$) momentum, the shock modification is weak, so the spectrum is more likely to be in a slightly nonlinear, almost TP regime. On the other hand, there is a putative indication from the electron radio emission that their spectrum may be close to $q_e \approx 1.75$, which could be the signature of a moderately nonlinear acceleration process. It should be remembered, however, that this is a global index across the W44 remnant. There are resolved bright filaments where a canonical $\alpha = -0.5$ spectrum, corresponding precisely to the TP parent electron spectrum with $q_e = 2$, is observed (Castelletti et al. 2007). Moreover, there are regions with the positive indices $\alpha \lesssim 0.4$ which cannot be indicative of a DSA process without corrections for subsequent spectral transformations such as an absorption by thermal electrons. These regions may contribute to the overall spectral hardening discussed above, thus mimicking the acceleration nonlinearity. Finally, secondary electrons give rise to the flattening of the radio spectrum as well (Uchiyama et al. 2010).

The above considerations somewhat weaken the radio data as a probe for the slope of the electron and (more importantly) for the proton spectrum. Therefore, the exact degree of nonlinearity of the acceleration remains unknown and one can consider both the TP and weakly NL regimes in calculations of the photon spectra, generated in $p-p$ collisions. Specifically, Malkov et al. (2005, 2011) calculate the π^0 production rate and the gamma-ray emissivity. In so doing, they adopt numerical recipe described in detail in (Kamae et al. 2006; Karlsson and Kamae 2008). The physical processes behind these calculations are (i) collisions of accelerated protons with the protons of the ambient gas resulting in $pp \to \pi^0$ reaction (ii) decay of π^0- mesons to generate an observable gamma emission spectrum.

An example of such calculations is shown in Fig.10. The best fit to the Fermi and AGILE data is provided by a TP energy distribution ($\propto E^{-2}$) below $p_{br} \simeq 7$GeV/c with the spectrum steepening by exactly one power above it. The spectrum steepening is perfectly consistent with the proton partial escape described above (with no parameters involved). For comparison, a weakly NL spectrum (guided by the inferred electron spectrum with $q_e \approx 1.75$, is also used for these calculations (dashed line in Fig.10), but its fit would require a somewhat stronger break ($\Delta q \gtrsim 1$) or a low momentum cut-off, i.e. at least one additional free parameter. It is seen that the mechanism for a break in the spectrum of shock accelerated protons suggested in (Malkov et al. 2005) provides a good fit to the recent (Abdo et al. 2010a) Fermi-LAT and AGILE (Giuliani et al. 2011) observations of the SNR W44. Of course, in assessing consistency of the suggested spectral break phenomenon with the observed spectrum, the errors in the data must be taken into account. The vertical error bars near the break at 2 GeV, are fairly small (comparable to the size of the symbols used to represent the data in Fig. 10). More significant appears to be the energy dispersion. However, in the most recent Fermi-LAT publication (see Ackermann et al. (2013) including the Supplementary Online Materi-

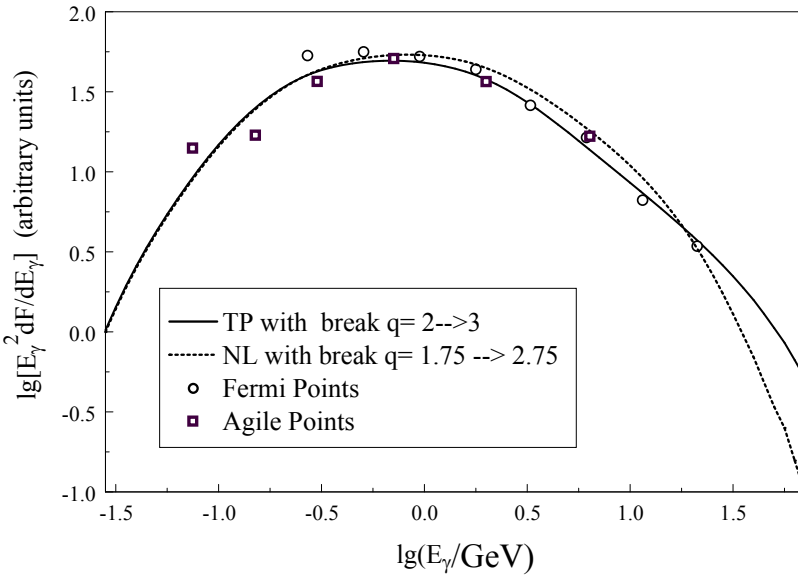

Fig. 10 Gamma radiation spectra. Photon spectra resulting from π^0 decay and calculated for two different parent proton spectra compared against the Fermi (circles) and AGILE (squares) data. Solid line: a test particle acceleration regime with the spectral index $q = 2$ below the break and $q = 3$ above the break at $p_{br} = 7GeV/c$. Dashed line: a moderately nonlinear acceleration regime corresponding to the spectrum with $q \simeq 1.75$ and $q \simeq 2.75$ below and above the break, respectively. Cut-offs are placed at 300 GeV for TP- and 100 GeV, for NL-spectrum. Fermi and AGILE data are adopted from (Abdo et al. 2010a; Giuliani et al. 2011), respectively. Both curves are well within the error bars of Fermi and AGILE (not shown for clarity), which, in turn, overlap (Giuliani et al. 2011).

als) the energy dispersion is estimated to be less than 5% for these energies, so that the broken power law is indeed consistent with the data.

Generally, spectral breaks offer a possible resolution to the well known problem that some nonlinear DSA models produce spectra which are considerably harder than a simple test particle spectrum, and these are not consistent with the gamma-ray observations of some of supernova remnants. However, the nonlinear spectrum – i.e., diverging in energy– exhausts the shock energy available for the acceleration as the cut-off momentum grows, so that a broken spectrum should form. Broken spectra are commonly observed and the old paradigm of a single power-law with an exponential upper cut-off is maladapted to the recent, greatly improved observations (Abdo et al. 2010b,2010a). Note, that the spectrum of the RX J1713.7-3946 (Aharonian et al. 2006) is also formally consistent with the environmental break mechanism presumably operating in W44 surrounding but with a higher $p_{br} \sim 10^3 GeV/c$ and thus with stronger acceleration nonlinearity (Malkov et al. 2005). However, this remnant expands into a rather complicated environment, so it is difficult to make the case for hadronic origin of the gamma-ray emission (Aharonian et al. 2004, 2006; Katz and Waxman 2008; Ellison et al. 2012). The important role of the W44 remnant for the problem of CR origin is that this particular remnant seems to be unlikely dominated by the lepton emission due to Bremsstrahlung and inverse Compton scattering (Abdo et al. 2010a; Uchiyama et al. 2010) thus favoring the hadronic origin of the gamma emission and bolstering the case for the SNR origin of galactic CRs.

8 Summary

Collisionless shocks are ubiquitous in astrophysical objects and are observed at all scales starting from the heliosphere and up to cosmological scale shocks observed in clusters of galaxies. Theoretical modeling of these shocks is challenging because shock relaxation process involves collective plasma oscillations producing long-lived highly nonequilibrium components. Straightforward numerical simulations are an extremely resource demanding task because of the very wide dynamical range of scales and time required to the resolve all of the long-lived components. Such task is even more difficult if neutral atoms and molecules are significant in the partially ionized media.

In this brief review we have discussed some observational appearance of collisionless shocks in partially ionized plasma, described the most important physical processes operating in the shocks and outlined the observational perspective of nonthermal components diagnostics of astrophysical collisionless shocks via multiwavelength observations.

Nonthermal components, i.e., energetic charged and neutral particles and fluctuating magnetic fields, can drastically modify the structure of the shock upstream providing both deceleration of the plasma flow and also efficient heating of ions and electrons. We argue that the processes of turbulence amplification and damping observed in the heliosphere may help to understand the microphysics of ion and electron heating by cosmic ray driven turbulence in the upstream regions of large scale collisionless shocks observed in the Galaxy and in clusters of galaxies. In turn, radiative signatures of the astrophysical shocks can be a unique way to study microscopic phenomena that can not be studied in the laboratory plasma on the Earth.

Hα line diagnostics of Balmer shocks provides valuable information on charge-exchange processes of the neutrals with both thermal and non-maxwellian plasma

components in the shock downstream. Nonthermal components may reduce the plasma temperature comparing to what is expected from the standard single-fluid Rankine-Hugoniot jump conditions for a particular shock velocity. In the case of radiative shocks this reduction would substantially modify the emission line spectrum coming from shock downstream and thus may serve as a valuable diagnostic tool for fast shocks interacting with clouds. The effect of neutrals on the MHD wave damping in the upstream of supernova shocks interacting with a molecular cloud may explain some spectral features in GeV energy regime, recently revealed by *Fermi* observations.

Acknowledgements A.M.B., J.C.R. and M.A.M. thank Andre Balogh and the ISSI staff for providing an inspiring atmosphere at the International Space Science Institute Workshop in Bern in 2012, which has led to the new collaboration. The authors thank the referee for a constructive report. A.M.B. and A.M.K. acknowledge support from the RAS Programs P 21 and OFN 16, and from the Ministry of Education and Science of Russian Federation (Agreement No. 8409, 2012). They performed the simulations at the Joint Supercomputing Centre (JSCC RAS) and the Supercomputing Centre at Ioffe Institute, St. Petersburg. M.M. acknowledges support by the Department of Energy, Grant No. DE-FG02-04ER54738. A.E.V. acknowledges support by NASA grants NNX09AC15G and NNX12AO73G.

References

Abdo AA, Ackermann M, Ajello M, Baldini L, et al. (2010a) Gamma-Ray Emission from the Shell of Supernova Remnant W44 Revealed by the Fermi LAT. Science 327:1103–1106

Abdo AA, Ackermann M, Ajello M, Baldini L, et al. (2010b) Observation of Supernova Remnant IC 443 with the Fermi Large Area Telescope. ApJ 712:459–468, 1002.2198

Achterberg A (1981) On the propagation of relativistic particles in a high beta plasma. A&A 98:161–172

Ackermann M, Ajello M, Allafort A, Baldini L, et al. (2013) Detection of the Characteristic Pion-Decay Signature in Supernova Remnants. Science 339:807–811

Aharonian F, Akhperjanian AG, Bazer-Bachi AR, Beilicke M, et al. (2006) A detailed spectral and morphological study of the gamma-ray supernova remnant RX J1713.7-3946 with HESS. A&A 449:223–242

Aharonian FA, Akhperjanian AG, Aye KM, Bazer-Bachi AR, et al. (2004) High-energy particle acceleration in the shell of a supernova remnant. Nat 432:75–77, arXiv:astro-ph/0411533

Aleksić J, Alvarez EA, Antonelli LA, Antoranz P, et al. (2012) Morphological and spectral properties of the W51 region measured with the MAGIC telescopes. A&A 541:A13, 1201.4074

Alexandrova O, Lacombe C, Mangeney A, Grappin R (2011) Fluid-like dissipation of magnetic turbulence at electron scales in the solar wind. ArXiv e-prints 1111.5649

Amato E, Blasi P (2006) Non-linear particle acceleration at non-relativistic shock waves in the presence of self-generated turbulence. MNRAS 371:1251–1258, arXiv:astro-ph/0606592

Bell AR (2004) Turbulent amplification of magnetic field and diffusive shock acceleration of cosmic rays. MNRAS 353:550–558

Blandford R, Eichler D (1987) Particle acceleration at astrophysical shocks: A theory of cosmic ray origin. Phys. Reports 154:1–75

Blasi P, Morlino G, Bandiera R, Amato E, et al. (2012) Collisionless Shocks in a Partially Ionized Medium. I. Neutral Return Flux and its Effects on Acceleration of Test Particles. ApJ 755:121, 1202.3080

Bode MF, Harman DJ, O'Brien TJ, Bond HE, et al. (2007) Hubble Space Telescope Imaging of the Expanding Nebular Remnant of the 2006 Outburst of the Recurrent Nova RS Ophiuchi. ApJ 665:L63–L66, 0706.2745

Boldyrev S, Perez JC (2012) Spectrum of Kinetic-Alfvén Turbulence. ApJ 758:L44, 1204.5809

Boulares A, Cox DP (1988) Application of cosmic-ray shock theories to the Cygnus Loop - an alternative model. ApJ 333:198–218

Bozhokin SV, Bykov AM (1994) Nonthermal particles in H I shells and supershells. Astronomy Letters 20:503–507

Braginskii SI (1965) Transport Processes in a Plasma. Reviews of Plasma Physics 1:205

Breech B, Matthaeus WH, Cranmer SR, Kasper JC, et al. (2009) Electron and proton heating by solar wind turbulence. Journal of Geophysical Research (Space Physics) 114(A13):A09103, 0907.4074

Brüggen M, Bykov A, Ryu D, Röttgering H (2012) Magnetic Fields, Relativistic Particles, and Shock Waves in Cluster Outskirts. Space Sci. Rev. 166:187–213, 1107.5223

Bykov AM (2004) Shocks and particle acceleration in SNRs: theoretical aspects. Advances in Space Research 33:366–375

Bykov AM (2005) Multi-fluid shocks in clusters of galaxies: Entropy, σ_v T, M T and L_X T scalings. Advances in Space Research 36:738–746, arXiv:astro-ph/0501575

Bykov AM, Chevalier RA, Ellison DC, Uvarov YA (2000) Nonthermal Emission from a Supernova Remnant in a Molecular Cloud. ApJ 538:203–216

Bykov AM, Dolag K, Durret F (2008) Cosmological Shock Waves. Space Sci. Rev. 134:119–140, 0801.0995

Bykov AM, Ellison DC, Renaud M (2012) Magnetic Fields in Cosmic Particle Acceleration Sources. Space Sci. Rev. 166:71–95, 1105.0130

Bykov AM, Osipov SM, Ellison DC (2011) Cosmic ray current driven turbulence in shocks with efficient particle acceleration: the oblique, long-wavelength mode instability. MNRAS 410:39–52, 1010.0408

Bykov AM, Toptygin IN (2005) Generation of Magnetic Fluctuations Near a Shock Front in a Partially Ionized Medium. Astronomy Letters 31:748–754

Carmona E (2011) Probing proton acceleration in W51C with MAGIC. In: International Cosmic Ray Conference, vol. 7 of International Cosmic Ray Conference, p. 114, 1110.0950

Castelletti G, Dubner G, Brogan C, Kassim NE (2007) The low-frequency radio emission and spectrum of the extended SNR W44: new VLA observations at 74 and 324 MHz. A&A 471:537–549

Chen CHK, Mallet A, Schekochihin AA, Horbury TS, et al. (2012) Three-dimensional Structure of Solar Wind Turbulence. ApJ 758:120, 1109.2558

Chevalier RA, Raymond JC (1978) Optical emission from a fast shock wave - The remnants of Tycho's supernova and SN 1006. ApJ 225:L27–L30

Cho J, Lazarian A (2004) The Anisotropy of Electron Magnetohydrodynamic Turbulence. ApJ 615:L41–L44, arXiv:astro-ph/0406595

Cowling TG (1976) Magnetohydrodynamics

Cranmer SR, van Ballegooijen AA (2012) Proton, Electron, and Ion Heating in the Fast Solar Wind from Nonlinear Coupling between Alfvénic and Fast-mode Turbulence. ApJ 754:92, 1205.4613

Dopita MA, Sutherland RS (1996) Spectral Signatures of Fast Shocks. I. Low-Density Model Grid. ApJS 102:161–+

Draine BT, McKee CF (1993) Theory of interstellar shocks. ARA&A 31:373–432

Drury LO (1983) An introduction to the theory of diffusive shock acceleration of energetic particles in tenuous plasmas. Reports on Progress in Physics 46:973–1027

Drury LO, Falle SAEG (1986) On the Stability of Shocks Modified by Particle Acceleration. MNRAS 223:353

Drury LOC, Duffy P, Kirk JG (1996) Limits on diffusive shock acceleration in dense and incompletely ionised media. A&A 309:1002–1010

Dupree TH (1966) A perturbation theory for strong plasma turbulence. Physics of Fluids 9(9):1773–1782

Ellison DC, Baring MG, Jones FC (1996) Nonlinear Particle Acceleration in Oblique Shocks. ApJ 473:1029, arXiv:astro-ph/9609182

Ellison DC, Bykov AM (2011) Gamma-ray Emission of Accelerated Particles Escaping a Supernova Remnant in a Molecular Cloud. ApJ 731:87, 1102.3885

Ellison DC, Slane P, Patnaude DJ, Bykov AM (2012) Core-collapse Model of Broadband Emission from SNR RX J1713.7-3946 with Thermal X-Rays and Gamma Rays from Escaping Cosmic Rays. ApJ 744:39, 1109.0874

Enomoto R, Tanimori T, Naito T, Yoshida T, et al. (2002) The acceleration of cosmic-ray protons in the supernova remnant RX J1713.7-3946. Nat 416:823–826

Evans A, Woodward CE, Helton LA, Gehrz RD, et al. (2007) Spitzer and Ground-based Infrared Observations of the 2006 Eruption of RS Ophiuchi. ApJ 663:L29–L32, 0705.2414

Farage CL, McGregor PJ, Dopita MA, Bicknell GV (2010) Optical IFU Observations of the Brightest Cluster Galaxy NGC 4696: The Case for a Minor Merger and Shock-excited Filaments. ApJ 724:267–284, 1009.3070

Fesen RA, Itoh H (1985) A two-dimensional spectrum of a nonradiative shock filament in the Cygnus Loop. ApJ 295:43–50
France K, McCray R, Penton SV, Kirshner RP, et al. (2011) HST-COS Observations of Hydrogen, Helium, Carbon, and Nitrogen Emission from the SN 1987A Reverse Shock. ApJ 743:186, 1111.1735
Fujita Y, Ohira Y, Yamazaki R (2013) Entropy at the Outskirts of Galaxy Clusters as Implications for Cosmological Cosmic-Ray Acceleration. ApJ 767:L4, 1303.1191
Gargaté L, Spitkovsky A (2012) Ion Acceleration in Non-relativistic Astrophysical Shocks. ApJ 744:67, 1107.0762
Gary SP, Chang O, Wang J (2012) Forward Cascade of Whistler Turbulence: Three-dimensional Particle-in-cell Simulations. ApJ 755:142
Ghavamian P, Laming JM, Rakowski CE (2007) A Physical Relationship between Electron-Proton Temperature Equilibration and Mach Number in Fast Collisionless Shocks. ApJ 654:L69–L72, arXiv:astro-ph/0611306
Ghavamian P, Raymond J, Hartigan P, Blair WP (2000) Evidence for Shock Precursors in Tycho's Supernova Remnant. ApJ 535:266–274
Ghavamian P, Raymond J, Smith RC, Hartigan P (2001) Balmer-dominated Spectra of Non-radiative Shocks in the Cygnus Loop, RCW 86, and Tycho Supernova Remnants. ApJ 547:995–1009, arXiv:astro-ph/0010496
Giannini T, Calzoletti L, Nisini B, Davis CJ, et al. (2008) Near-infrared, IFU spectroscopy unravels the bow-shock HH99B. A&A 481:123–139, 0801.1633
Giuliani A, Cardillo M, Tavani M, Fukui Y, et al. (2011) Neutral Pion Emission from Accelerated Protons in the Supernova Remnant W44. ApJ 742:L30, 1111.4868
Gloeckler G, Geiss J (2001) Heliospheric and Interstellar Phenomena Deduced From Pickup ion Observations. Space Sci. Rev. 97:169–181
Goldreich P, Sridhar S (1995) Toward a theory of interstellar turbulence. 2: Strong alfvenic turbulence. ApJ 438:763–775
Hartigan P, Raymond J, Hartmann L (1987) Radiative bow shock models of Herbig-Haro objects. ApJ 316:323–348
Helder EA, Kosenko D, Vink J (2010) Cosmic-ray Acceleration Efficiency versus Temperature Equilibration: The Case of SNR 0509-67.5. ApJ 719:L140–L144, 1007.3138
Helder EA, Vink J, Bassa CG, Bamba A, et al. (2009) Measuring the Cosmic-Ray Acceleration Efficiency of a Supernova Remnant. Science 325:719–, 0906.4553
Helder EA, Vink J, Bykov AM, Ohira Y, et al. (2012) Observational Signatures of Particle Acceleration in Supernova Remnants. Space Sci. Rev. 173:369–431, 1206.1593
Heng K (2010) Balmer-Dominated Shocks: A Concise Review. PASA 27:23–44, 0908.4080
Heng K, McCray R (2007) Balmer-dominated Shocks Revisited. ApJ 654:923–937, arXiv:astro-ph/0609331
Heng K, van Adelsberg M, McCray R, Raymond JC (2007) The Transition Zone in Balmer-dominated Shocks. ApJ 668:275–284, 0705.2619
Hester JJ, Raymond JC, Blair WP (1994) The Balmer-dominated northeast limb of the Cygnus loop supernova remnant. ApJ 420:721–745
Howes GG (2010) A prescription for the turbulent heating of astrophysical plasmas. MNRAS 409:L104–L108, 1009.4212
Howes GG, Cowley SC, Dorland W, Hammett GW, et al. (2006) Astrophysical Gyrokinetics: Basic Equations and Linear Theory. ApJ 651:590–614, arXiv:astro-ph/0511812
Inoue T, Yamazaki R, Inutsuka Si, Fukui Y (2012) Toward Understanding the Cosmic-Ray Acceleration at Young Supernova Remnants Interacting with Interstellar Clouds: Possible Applications to RX J1713.7-3946. ApJ 744:71, 1106.3080
Jones FC, Ellison DC (1991) The plasma physics of shock acceleration. Space Sci. Rev. 58:259–346
Kamae T, Karlsson N, Mizuno T, Abe T, et al. (2006) Parameterization of gamma, e+/-, and Neutrino Spectra Produced by p-p Interaction in Astronomical Environments. ApJ 647:692–708
Karlsson N, Kamae T (2008) Parameterization of the Angular Distribution of Gamma Rays Produced by p-p Interaction in Astronomical Environments. ApJ 674:278–285
Katz B, Waxman E (2008) In which shell-type SNRs should we look for gamma-rays and neutrinos from P P collisions? Journal of Cosmology and Astro-Particle Physics 1:1–29
Kulsrud R, Pearce WP (1969) The Effect of Wave-Particle Interactions on the Propagation of Cosmic Rays. ApJ 156:445–469

Leamon RJ, Smith CW, Ness NF, Matthaeus WH, et al. (1998) Observational constraints on the dynamics of the interplanetary magnetic field dissipation range. J. Geophys. Res. 103:4775

Lee JJ, Koo BC, Raymond J, Ghavamian P, et al. (2007) Subaru HDS Observations of a Balmer-dominated Shock in Tycho's Supernova Remnant. ApJ 659:L133–L136, 0704.1094

Lee JJ, Raymond JC, Park S, Blair WP, et al. (2010) Resolved Shock Structure of the Balmer-dominated Filaments in Tycho's Supernova Remnant: Cosmic-ray Precursor? ApJ 715:L146–L149, 1005.3296

Lim AJ, Raga AC (1996) A distribution function calculation of the Hα profiles of high-velocity shocks - II. The broad component neutral precursor. MNRAS 280:103–114

Malkov MA (1997) Analytic Solution for Nonlinear Shock Acceleration in the Bohm Limit. ApJ 485:638, arXiv:astro-ph/9707152

Malkov MA, Diamond PH, Sagdeev RZ (2005) On the Gamma-Ray Spectra Radiated by Protons Accelerated in Supernova Remnant Shocks near Molecular Clouds: The case of Supernova Remnant RX J1713.7-3946. ApJ 624:L37–L40

Malkov MA, Diamond PH, Sagdeev RZ (2011) Mechanism for spectral break in cosmic ray proton spectrum of supernova remnant W44. Nature Communications 2/1195, 1004.4714

Malkov MA, Drury LO (2001) Nonlinear theory of diffusive acceleration of particles by shock waves. Reports on Progress in Physics 64:429–481

Malkov MA, Sagdeev RZ, Diamond PH (2012) Magnetic and Density Spikes in Cosmic-Ray Shock Precursors. ApJ 748:L32, 1110.0257

Marcowith A, Lemoine M, Pelletier G (2006) Turbulence and particle acceleration in collisionless supernovae remnant shocks. II. Cosmic-ray transport. A&A 453:193–202, arXiv:astro-ph/0603462

Massi F, Codella C, Brand J, di Fabrizio L, et al. (2008) The low-mass YSO CB230-A: investigating the protostar and its jet with NIR spectroscopy and Spitzer observations. A&A 490:1079–1091, 0809.1591

McComas DJ, Allegrini F, Bochsler P, Bzowski M, et al. (2009) Global Observations of the Interstellar Interaction from the Interstellar Boundary Explorer (IBEX). Science 326:959–

McKee CF, Hollenbach DJ (1980) Interstellar shock waves. ARA&A 18:219–262

Mihalas D, Mihalas BW (1984) Foundations of radiation hydrodynamics. New York, Oxford University Press, 1984, 731 p.

Mithaiwala M, Rudakov L, Crabtree C, Ganguli G (2012) Co-existence of whistler waves with kinetic Alfven wave turbulence for the high-beta solar wind plasma. Physics of Plasmas 19(10):102 902, 1208.0623

Monin AS, Iaglom AM (1975) Statistical fluid mechanics: Mechanics of turbulence. Volume 2 /revised and enlarged edition/

Morlino G, Bandiera R, Blasi P, Amato E (2012a) Collisionless Shocks in a Partially Ionized Medium. II. Balmer Emission. ApJ 760:137, 1210.4296

Morlino G, Blasi P, Bandiera R, Amato E, et al. (2012b) Collisionless shocks in a partially ionized medium: III. Efficient cosmic ray acceleration. ArXiv e-prints 1211.6148

Morse JA, Blair WP, Dopita MA, Hughes JP, et al. (1996) Hubble Space Telescope Observations of Oxygen-Rich Supernova Remnants in the Magellanic Cloud. I. Narrow-Band Imaging of N132D in the LMC. AJ112:509

Nakano T (1984) Contraction of magnetic interstellar clouds. Fundamentals of Cosmic Physics 9:139–231

Nikolić S, van de Ven G, Heng K, Kupko D, et al. (2013) An Integral View of Fast Shocks around Supernova 1006. ArXiv e-prints 1302.4328

O'C Drury L, Duffy P, Kirk JG (1996) Limits on diffusive shock acceleration in dense and incompletely ionised media. A&A 309:1002–1010, arXiv:astro-ph/9510066

Ohira Y (2012) Effects of Leakage Neutral Particles on Shocks. ApJ 758:97, 1202.4620

Ohira Y, Takahara F (2010) Effects of Neutral Particles on Modified Shocks at Supernova Remnants. ApJ 721:L43–L47, 0912.2859

Ohira Y, Terasawa T, Takahara F (2009) Plasma Instabilities as a Result of Charge Exchange in the Downstream Region of Supernova Remnant Shocks. ApJ 703:L59–L62, 0908.3369

Petrosyan A, Balogh A, Goldstein ML, Léorat J, et al. (2010) Turbulence in the Solar Atmosphere and Solar Wind. Space Sci. Rev. 156:135–238

Pierrard V, Lazar M (2010) Kappa Distributions: Theory and Applications in Space Plasmas. Solar Phys.267:153–174, 1003.3532

Quataert E (1998) Particle Heating by Alfvenic Turbulence in Hot Accretion Flows. ApJ 500:978, arXiv:astro-ph/9710127

Quataert E, Gruzinov A (1999) Turbulence and Particle Heating in Advection-dominated Accretion Flows. ApJ 520:248–255, arXiv:astro-ph/9803112

Rakowski CE, Laming JM, Ghavamian P (2008) The Heating of Thermal Electrons in Fast Collisionless Shocks: The Integral Role of Cosmic Rays. ApJ 684:348–357, 0805.3084

Ramos JJ (2011) Fluid and drift-kinetic description of a magnetized plasma with low collisionality and slow dynamics orderings. II. Ion theory. Physics of Plasmas 18(10):102 506

Raymond JC (1979) Shock waves in the interstellar medium. ApJS 39:1–27

Raymond JC (1991) Supernova-remnant shock waves close up. PASP 103:781–786

Raymond JC, Hartmann L, Hartigan P (1988a) Improved bow shock models for Herbig-Haro objects - Application to HH 2A-prime. ApJ 326:323–333

Raymond JC, Hester JJ, Cox D, Blair WP, et al. (1988b) Spatial and spectral interpretation of a bright filament in the Cygnus Loop. ApJ 324:869–892

Raymond JC, Isenberg PA, Laming JM (2008) Non-Maxwellian Proton Velocity Distributions in Nonradiative Shocks. ApJ 682:408–415, 0804.3808

Raymond JC, Vink J, Helder EA, de Laat A (2011) Effects of Neutral Hydrogen on Cosmic-ray Precursors in Supernova Remnant Shock Waves. ApJ 731:L14, 1103.3211

Raymond JC, Winkler PF, Blair WP, Lee JJ, et al. (2010) Non-Maxwellian Hα Profiles in Tycho's Supernova Remnant. ApJ 712:901–907

Reach WT, Rho J, Jarrett TH (2005) Shocked Molecular Gas in the Supernova Remnants W28 and W44: Near-Infrared and Millimeter-Wave Observations. ApJ 618:297–320

Reville B, Kirk JG, Duffy P, O'Sullivan S (2007) A cosmic ray current-driven instability in partially ionised media. A&A 475:435–439, 0707.3743

Reville B, Kirk JG, Duffy P, O'Sullivan S (2008) Environmental Limits on the Nonresonant Cosmic-Ray Current-Driven Instability. International Journal of Modern Physics D 17:1795–1801

Sahraoui F, Goldstein ML, Robert P, Khotyaintsev YV (2009) Evidence of a Cascade and Dissipation of Solar-Wind Turbulence at the Electron Gyroscale. Physical Review Letters 102(23):231102

Saito S, Gary SP (2012) Beta dependence of electron heating in decaying whistler turbulence: Particle-in-cell simulations. Phys of Plasmas 19:012 312

Schekochihin AA, Cowley SC, Dorland W, Hammett GW, et al. (2009) Astrophysical Gyrokinetics: Kinetic and Fluid Turbulent Cascades in Magnetized Weakly Collisional Plasmas. ApJS 182:310–377, 0704.0044

Schure KM, Bell AR, O'C Drury L, Bykov AM (2012) Diffusive Shock Acceleration and Magnetic Field Amplification. Space Sci. Rev. 173:491–519, 1203.1637

Shull JM, McKee CF (1979) Theoretical models of interstellar shocks. I - Radiative transfer and UV precursors. ApJ 227:131–149

Skilling J (1975) Cosmic ray streaming. I - Effect of Alfven waves on particles. MNRAS 172:557–566

Smith RC, Raymond JC, Laming JM (1994) High-resolution spectroscopy of Balmer-dominated shocks in the Large Magellanic Cloud. ApJ 420:286–293

Sollerman J, Ghavamian P, Lundqvist P, Smith RC (2003) High resolution spectroscopy of Balmer-dominated shocks in the RCW 86, Kepler and SN 1006 supernova remnants. A&A 407:249–257, arXiv:astro-ph/0306196

Spitzer L (1978) Physical processes in the interstellar medium

Tatischeff V, Hernanz M (2007) Evidence for Nonlinear Diffusive Shock Acceleration of Cosmic Rays in the 2006 Outburst of the Recurrent Nova RS Ophiuchi. ApJ 663:L101–L104, 0705.4422

Teşileanu O, Massaglia S, Mignone A, Bodo G, et al. (2009) Time-dependent MHD shocks and line intensity ratios in the HH 30 jet: a focus on cooling function and numerical resolution. A&A 507:581–588, 0910.1225

Uchiyama Y, Blandford RD, Funk S, Tajima H, et al. (2010) Gamma-ray Emission from Crushed Clouds in Supernova Remnants. ApJ 723:L122–L126

van Adelsberg M, Heng K, McCray R, Raymond JC (2008) Spatial Structure and Collisionless Electron Heating in Balmer-dominated Shocks. ApJ 689:1089–1104, 0803.2521

Verma MK (2004) Statistical theory of magnetohydrodynamic turbulence: recent results. Phys. Reports 401:229–380, arXiv:nlin/0404043

Vink J (2012) Supernova remnants: the X-ray perspective. Astron. Astroph. Reviews 20:49, 1112.0576

Vink J, Yamazaki R, Helder EA, Schure KM (2010) The Relation Between Post-shock Temperature, Cosmic-ray Pressure, and Cosmic-ray Escape for Non-relativistic Shocks. ApJ 722:1727–1734, 1008.4367

Vladimirov AE, Bykov AM, Ellison DC (2008) Turbulence Dissipation and Particle Injection in Nonlinear Diffusive Shock Acceleration with Magnetic Field Amplification. ApJ 688:1084–1101, 0807.1321

Vladimirov AE, Bykov AM, Ellison DC (2009) Spectra of Magnetic Fluctuations and Relativistic Particles Produced by a Nonresonant Wave Instability in Supernova Remnant Shocks. ApJ 703:L29–L32, 0908.2602

Völk HJ, Morfill GE, Forman MA (1981) The effect of losses on acceleration of energetic particles by diffusive scattering through shock waves. ApJ 249:161–175

Wagner AY, Lee JJ, Raymond JC, Hartquist TW, et al. (2009) A Cosmic-Ray Precursor Model for a Balmer-Dominated Shock in Tycho's Supernova Remnant. ApJ 690:1412–1423, 0809.2504

Williams LL, Zank GP (1994) Effect of magnetic field geometry on the wave signature of the pickup of interstellar neutrals. J. Geophys. Res. 99:19 229

Zhou Y (2010) Renormalization group theory for fluid and plasma turbulence. Phys. Reports 488:1–49

Zhou Y, Matthaeus WH (1990) Models of inertial range spectra of interplanetary magnetohydrodynamic turbulence. J. Geophys. Res. 95:14 881–14 892

Zweibel EG, Shull JM (1982) Confinement of cosmic rays in molecular clouds. ApJ 259:859–868